nagra
National Cooperative for the
Disposal of Radioactive Waste

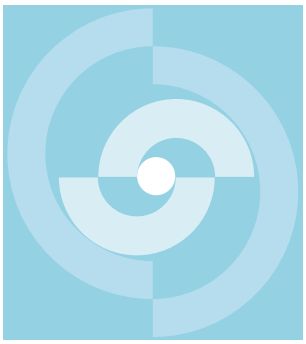

TECHNICAL REPORT 01-04

Calculations of the Temperature Evolution of a Repository for Spent Fuel, Vitrified High-Level Waste and Intermediate Level Waste in Opalinus Clay

October 2002

L.H. Johnson, M. Niemeyer, G. Klubertanz
P. Siegel and P. Gribi

Hardstrasse 73, CH-5430 Wettingen/Switzerland, Telephone +41-56-437 11 11

nagra
National Cooperative for the
Disposal of Radioactive Waste

TECHNICAL REPORT 01-04

Calculations of the Temperature Evolution of a Repository for Spent Fuel, Vitrified High-Level Waste and Intermediate Level Waste in Opalinus Clay

October 2002

L.H. Johnson[1)], M. Niemeyer[2)], G. Klubertanz[2)]
P. Siegel[2)] and P. Gribi[3)]

[1)] Nagra, Wettingen

[2)] Colenco Power Engineering AG, Baden

[3)] Vibro-Consult Ltd., Brugg

Hardstrasse 73, CH-5430 Wettingen/Switzerland, Telephone +41-56-437 11 11

This report was prepared on behalf of Nagra. The viewpoints presented and conclusions reached are those of the author(s) and do not necessarily represent those of Nagra.

ISSN 1015-2636

Abstract

Thermal evolution is an important aspect of the performance of a repository for nuclear waste, because elevated temperatures affect many processes influencing the behaviour of engineered barrier systems and the host rock. The thermal evolution of a repository for spent fuel, high-level waste (HLW) and intermediate level waste (ILW) has been evaluated. The repository is assumed to be located at a depth of 650 m in the Opalinus Clay formation in northern Switzerland. The disposal system consists of spent fuel and HLW, encapsulated within steel canisters that are emplaced within horizontal tunnels, with the space between the canisters and the surrounding rock backfilled with bentonite. Waste emplacement tunnels are spaced 40 m apart. Concrete containers of ILW are placed in separate emplacement tunnels, with the void space around the containers filled with cementitious mortar.

The initial heat output of the waste and the rate of its decrease with time due to radioactive decay depends on the nature of the waste. For the case of spent fuel, some canisters contain only UO_2 assemblies, while others contain both UO_2 and MOX (mixed oxide) fuel assemblies. The initial heat output of both canister types is restricted to 1500 W/canister, but the time-dependent heat output of the UO_2/MOX canisters declines more slowly, as a result of significantly higher Pu content. For HLW canisters, the initial heat output is ~700 W and it decreases more rapidly than is the case for spent fuel, because of the low actinide content of HLW.

The temperature evolution of the engineered barrier system and surrounding rock is simulated using a finite-element model, using reference data for the thermal properties of spent fuel, HLW, bentonite backfill and Opalinus Clay. The results show that the surface temperatures of both the HLW and spent fuel canisters reach a maximum value of ~150°C within a few years after emplacement, although the HLW canister temperature decreases much more rapidly than for the case of spent fuel canisters. The temperatures within the bentonite depend strongly on the assumptions regarding its water content. For the expected low water inflow rates in a repository in low permeability Opalinus Clay, the bentonite has a low thermal conductivity and the temperature at the point midway between spent fuel canisters and the bentonite/host rock interface will reach a maximum of ~110°C. For HLW canisters, the mid-point of the bentonite will not exceed 100°C. Host rock temperatures remain below ~90°C at all times. In the unlikely event of a more rapid rate of inflow of water from the Opalinus Clay, the bentonite thermal conductivity is significantly greater and temperatures at the canister/bentonite interface and throughout the bentonite are markedly reduced.

For the case of ILW tunnels, a boundary element model is used to calculate temperature evolution, taking into consideration the hydration heat of the concrete mortar and radioactive decay. It is found that the maximum temperature reached within the engineered barrier system is ~50°C, about 12°C more than the ambient temperature in the Opalinus Clay at a depth of 650 m.

Zusammenfassung

Die thermische Entwicklung ist ein wichtiger Faktor für das Systemverhalten eines Lagers für radioaktive Abfälle, weil erhöhte Temperaturen viele Prozesse beeinflussen, welche sich auf das Verhalten der technischen Barrieren und des Wirtgesteins auswirken. Im vorliegenden Bericht wird die thermische Entwicklung eines Lagers für abgebrannte Brennelemente, verglaste hochaktive Abfälle (HAA) und langlebige mittelaktive Abfälle (LMA) bewertet. Dabei wird angenommen, dass sich das Lager in einer Tiefe von 650 m im Opalinuston der Nordschweiz befindet. Das Lagersystem besteht aus abgebrannten Brennelementen und HAA, die in Stahlbehältern eingeschlossen und in horizontalen Stollen eingelagert werden. Der Hohlraum zwischen Behältern und umgebendem Gestein wird mit Bentonit verfüllt. Die Einlagerungsstollen weisen einen Abstand von 40 m auf. Betoncontainer mit LMA werden in separaten Tunnels eingelagert, wobei der Hohlraum um die Container mit Zementmörtel verfüllt wird.

Die anfängliche Wärmeproduktion der Abfälle und deren Abnahme im Laufe der Zeit infolge radioaktiven Zerfalls hängen von der Beschaffenheit des Abfalls ab. Einige Behälter enthalten ausschliesslich UO_2-Brennelemente, während andere Behälter sowohl UO_2- als auch MOX (Mixed Oxide)-Brennelemente enthalten. Die anfängliche Wärmeproduktion beider Behältertypen ist begrenzt auf 1500 W/Behälter, wobei die Wärmeproduktion der UO_2/MOX-Behälter aufgrund des signifikant höheren Pu-Gehalts langsamer abnimmt. Die Wärmeproduktion der HAA-Behälter beträgt am Anfang ca. 700 W/Behälter und nimmt aufgrund des niedrigen Aktinidengehalts schneller ab als diejenige von abgebrannten Brennelementen.

Die Temperaturentwicklung der technischen Barrieren und des umgebenden Gesteins wurde mittels eines Finite-Element-Modells simuliert, unter Verwendung von Referenzdaten für die thermischen Eigenschaften von abgebrannten Brennelementen, HAA, Bentonit und Opalinuston. Die Resultate zeigen, dass die Oberflächentemperatur sowohl der Brennelement- als auch der HAA-Behälter innerhalb weniger Jahre nach Einlagerung ein Maximum von ca. 150°C erreicht. Die HAA-Behältertemperatur nimmt allerdings viel schneller ab als diejenige der Brennelement-Behälter. Die Temperaturen im Bentonit hängen stark vom angenommenen Wassergehalt ab. Im Falle der erwartet geringen Wasserzuflussraten aus dem geringdurchlässigen Opalinuston in das Lager weist Bentonit eine geringe thermische Leitfähigkeit auf und die Temperatur in der Mitte zwischen den Brennelement-Behältern und dem Wirtgestein beträgt maximal ca. 110°C. Im Falle der HAA-Behälter bleibt die Temperatur in der Bentonitmitte unter ca. 100°C. Die Temperaturen im Wirtgestein bleiben für alle Zeiten unter ca. 90°C. Im unwahrscheinlichen Fall eines erhöhten Wasserzuflusses aus dem Opalinuston fällt die thermische Leitfähigkeit von Bentonit signifikant höher aus und die Temperaturen an der Behälteroberfläche und im Bentonit sind deutlich vermindert.

Für die Berechnung der Temperaturentwicklung in den LMA-Tunnels wurde ein Boundary-Element-Modell verwendet, das die Wärmeentwicklung infolge Hydratation und radioaktiven Zerfalls berücksichtigt. Die Resultate zeigen, dass die Temperatur innerhalb des technischen Barrierensystems maximal ca. 50°C erreicht, 12°C über der Umgebungstemperatur im Opalinuston in 650 m Tiefe.

Résumé

L'évolution du dégagement thermique joue un rôle important dans l'évaluation d'un site destiné au stockage de déchets radioactifs. En effet, des températures élevées affectent de nombreux processus qui gouvernent le comportement du système de barrières ouvragées et celui de la roche d'accueil. Cette étude concerne l'évolution thermique d'un site de stockage pour combustible irradié et déchets de haute (DHA) et de moyenne activité (DMA). On suppose que le site est situé à une profondeur de 650 m dans la formation d'argiles à Opalinus du nord de la Suisse. Le système d'entreposage est composé de combustible irradié et de DHA, conditionnés dans des conteneurs en acier, eux-mêmes placés dans des galeries horizontales. De la bentonite est utilisée pour combler l'espace existant entre les colis et la roche environnante. Les galeries contenant les déchets sont espacées de 40 m. Les conteneurs en béton pour DMA sont placés dans des galeries séparées, l'espace entre les conteneurs étant rempli à l'aide d'un mortier de ciment.

Le dégagement thermique initial et sa diminution progressive due à la décroissance radioactive sont dépendants de la nature des déchets. Dans le cas du combustible irradié, certains colis ne renferment que du combustible UO_2, tandis que d'autres contiennent à la fois du combustible UO_2 et MOX (Mixed Oxide). Le dégagement thermique initial des deux types de colis est limité à 1500 W/conteneur, mais décroît plus lentement pour les colis UO_2/MOX, en raison de la présence de Pu en quantités plus importantes. Pour les conteneurs de DHA, le dégagement thermique initial est d'environ 700 W et décroît plus rapidement que dans le cas du combustible irradié, à cause de la faible quantité d'actinides présents dans les DHA.

L'évolution thermique du système de barrières ouvragées et de la roche environnante a été simulée par le biais d'un modèle à éléments finis, en faisant appel à des données de référence pour les propriétés thermiques du combustible irradié, des DHA, de la bentonite utilisée pour le remplissage et des argiles à Opalinus. Les résultats montrent que, tant pour les DHA que pour le combustible irradié, la température à la surface des conteneurs atteint une valeur maximum d'environ 150°C quelques années après leur mise en place, en précisant que la température des colis de DHA décroît beaucoup plus rapidement que celle des conteneurs de combustible irradié. La température de la bentonite est en rapport étroit avec la teneur en eau qui lui est attribuée. Si l'on suppose que l'afflux d'eau en provenance de la couche d'argile à Opalinus, peu perméable, sera faible, le taux de conductivité thermique de la bentonite sera bas et la température mesurée à égale distance du colis de combustible irradié et du point de contact entre la bentonite et la roche d'accueil atteindra un maximum d'environ 110°C. Pour les colis de DHA, le point situé au centre du remplissage de bentonite ne dépassera pas 100°C. Les températures de la roche d'accueil restent inférieures à environ 90°C dans tous les cas. Dans l'éventualité, peu probable, d'un afflux d'eau plus rapide en provenance de l'argile à Opalinus, la conductivité thermique de la bentonite augmentera de façon notoire et les températures au point de contact conteneur/bentonite et dans la bentonite elle-même baisseront sensiblement

Dans le cas des galeries contenant les DMA, un modèle à éléments frontières a été utilisé pour calculer l'évolution thermique, prenant en considération la chaleur générée par l'hydratation du béton et la décroissance radioactive. La température maximum atteinte à l'intérieur du système de barrières ouvragées est d'environ 50°C, c'est-à-dire qu'elle est supérieure d'environ 12°C à la température régnant normalement dans les argiles à Opalinus à une profondeur de 650 m.

Table of Contents

List of Tables

List of Figures

List of Appendices

1 Introduction

In Switzerland, management of radioactive waste is the responsibility of those who produce it. In terms of Swiss law, this means permanent, safe disposal in engineered geologic repositories. The waste producers include the electrical utilities, responsible for operating the nuclear power plants, and the Swiss federal government, responsible for radioactive wastes from medicine, industry and research. Nagra, the National Co-operative for the Disposal of Radioactive Waste, was established by the producers to develop the technology for achieving safe disposal.

The nuclear waste management concept in Switzerland is based on the principle of two types of repository for wastes with different radiotoxicity levels, the use of multiple safety barriers, the priority of long-term safety over other requirements and a long period of storage for heat-generating high-level waste and spent fuel before final disposal.

Two host rock options are under consideration for the disposal of spent fuel, HLW and long-lived intermediate-level waste: the crystalline basement rock and the Opalinus Clay of Northern Switzerland. Studies of the crystalline rock option are largely complete and the present focus of studies is the Opalinus Clay in the Zürcher Weinland region. The present study examines the thermal behaviour of a repository in the Opalinus Clay.

The decay of radioactive waste generates heat, which will affect temperatures within the engineered barrier system (EBS) and surrounding rock in a repository containing nuclear wastes. Temperature affects many processes occurring in the repository, thus, during the repository design and safety assessment process, it is necessary to determine an appropriate density of emplacement of heat-generating wastes and examine the resultant time-dependent temperature distributions and their implications. Temperature distributions in the EBS for a repository containing vitrified high level waste (HLW) in crystalline rock were calculated for the Kristallin-I study (NAGRA 1994). More recently, SATO et al. (1998) calculated temperature distributions for repository designs for disposal of spent fuel (SF) in crystalline rock and Opalinus Clay. The latter study provided guidance on repository design and the maximum thermal output of spent fuel canisters.

The present study extends this work by calculating temperature evolution in a repository for SF, HLW and intermediate-level waste (ILW) in Opalinus Clay. The repository, based on the reference design of NOLD (2000), is assumed to be located at a depth of 650 m. It consists of parallel tunnels for spent fuel and high level waste glass, with both waste types contained in long-lived canisters, as well as three short tunnels for intermediate level wastes solidified in concrete waste packages, located in a separate part of the repository. The temperature distribution within the EBS of the HLW and SF emplacement tunnels and in the surrounding rock is calculated using a finite-element model. The temperature evolution of the rock surrounding emplacement tunnels for ILW is also evaluated, using a boundary element model.

2 Thermal Constraints on Repository Design

The temperature constraints for the various components of the EBS are discussed here, to clarify which constraints are the most restrictive in terms of repository thermal loading.

HLW – The temperature of HLW glass should remain below ~500°C (LUTZE 1988), to avoid devitrification, which might affect glass corrosion rates after canister failure. For a canister surrounded by bentonite (canister surface temperature ~150°C), glass temperatures reach ~200°C (NAGRA 1994), thus there is a large margin of safety.

SF – Fuel cladding temperatures should remain below ~350°C to avoid any possibility of creep rupture. This represents a criterion for interim storage of spent fuel. No calculations of temperature distributions within the Nagra steel canister for SF have been performed, but calculations for the SKB Cu/steel canister, which has a design similar to the Nagra canister, containing 12 BWR elements with a total heat output of 2855 W, have been performed by RENSTRÖM (1997). Maximum temperatures of ~400°C were calculated, from which it can be reasonably inferred that fuel cladding temperatures would be well below 350°C for a Nagra canister of similar mass and approximately the same mass of fuel, but with a much lower heat output of 1500 W at the time of emplacement. As a result, fuel cladding temperatures are expected to be much lower than the creep rupture temperature threshold.

Steel Canister - Based on various assessments of the corrosion performance of carbon steel canisters (NAGRA 1994, JNC 2000), there does not appear to be a requirement for a temperature limit for the canister surface, such as has been defined for Cu canisters (WERME 1998).

Bentonite - It is frequently assumed that the most restrictive thermal constraint for repository design relates to the maximum temperatures to be experienced by the bentonite barrier immediately around the canister. In the Kristallin-I study (NAGRA 1994), it was noted that, to assure high swelling capacity, it is desirable that a significant thickness of bentonite does not experience temperatures above 100°C. Short term processes that may affect bentonite performance include cementation as a result of exposure to hot unsaturated conditions in the period shortly after emplacement of the bentonite (COUTURE 1985), or by precipitation of soluble salts that migrate towards the canister (PUSCH et al. 1992). Little illitisation is expected to occur because significant alteration of smectite to illite requires unfavourable groundwater chemistry ($[K^+] \geq 10^{-2}$ mol/L) and temperatures of > 100°C for tens of thousands of years (PUSCH and MADSEN, 1995). Neither of these conditions apply for the case of a spent fuel repository in Opalinus Clay. In the case of the Swedish repository design, the requirement is that the temperature at the bentonite/canister interface remains below 100°C to limit boiling in the unsaturated phase (SKB 1999) which can concentrate soluble salts at the surface of the canister. This is principally a criterion related to corrosion performance of copper canisters (RAIKO 1996, WERME 1998), but also relates to preventing potential alteration of the bentonite during the unsaturated phase immediately after canister emplacement. For a repository in Opalinus Clay, with a low water inflow rate (the hydraulic conductivity of Opalinus Clay is $< 10^{-13}$ ms^{-1} (NAGRA 2001)) and the low moisture content of bentonite at emplacement (~ 2%, see Section 5), vapour phase cementation of bentonite at temperatures above 100°C may be the greatest concern regarding potential loss of swelling capacity. Exposure to such conditions has been shown to degrade the swelling properties of uncompacted bentonite (COUTURE 1985), although it has little effect on the swelling of dense bentonite (OSCARSON & DIXON 1990). A study by PUSCH (2000) has shown that the swelling and hydraulic properties of dense bentonite are not significantly affected by exposure to water vapour at 110°C. For the case of dense bentonite pellets, the backfill material considered in the Opalinus Clay study (NOLD

2000), no significant loss of swelling capacity occurs at 125°C, although there is a reduction by a factor of two at 150°C (PUSCH et al. 2002). These findings suggest that the swelling properties of the outer half of the bentonite can be assured if temperatures in this region do not exceed 125°C.

3 Summary of Main Findings of Previous Nagra Studies of Temperature Evolution in a SF/HLWRepository

Calculations of temperature evolution in the EBS for the case of high-level waste (HLW) canisters emplaced in large diameter tunnels in crystalline rock were reported in Kristallin-I (NAGRA 1994). The maximum canister surface temperature was ~150°C, with peak temperatures at the midpoint of the bentonite of ~100°C.

The calculations of SATO et al. (1998) used preliminary data for decay heat of spent fuel canisters and thermal properties of Opalinus Clay. Temperature evolution was calculated for tunnel spacings of 20 and 40 m and a separation between canisters in the tunnels of 3 m. Another important parameter examined was the heat output of spent fuel canisters at the time of emplacement. For canisters with a heat output of 1500 W at the time of emplacement as compared to 1000 W, peak temperatures in the middle of the bentonite increased from 75 to 95°C. In addition, a study by MCGINNES & SCHNEIDER (1998) for the case of canisters containing fuel assemblies of various burn-ups, including MOX and high burnup UO_2 fuel, showed that, in most cases, mixing of various combinations of fuel assemblies, e.g., combining 1 MOX assembly with 3 UO_2 assemblies, will ensure that a 1500 W limit is not exceeded (see Section 5). Based on all these calculations, a maximum heat output for SF canisters of 1500 W at the time of emplacement, a tunnel spacing of 40 m and a separation between spent fuel canisters of 3 m were selected for repository design. However, all the temperature calculations for spent fuel canisters were based on preliminary data for thermal properties of Opalinus Clay and bentonite, and on preliminary decay heat curves for spent fuel canisters. The present study uses updated data for decay heat of SF, HLW and ILW. In addition, new data for the thermal properties of Opalinus Clay have been derived from measurements in the borehole at Benken, and the thermal properties of granular bentonite backfill have been re-evaluated, based on information from the literature.

4 Repository Layout and Engineered Barrier System

Overall Repository Layout

The repository is assumed to be located at a depth of 650 m in the Opalinus Clay formation. The overall repository layout is shown in Fig. 1 (NOLD 2000). It consists of a large number of disposal tunnels, spaced 40 m apart, for SF and HLW, in which the canisters are emplaced horizontally. The void around and between canisters is filled with a mixture of dense bentonite pellets and bentonite powder, while the canisters rest on blocks of precompacted bentonite (Fig. 2). The tunnels have a diameter of 2.5 m. For the temperature evolution calculations, a simplified representation is adopted, with a bentonite pellet/powder mixture of uniform density surrounding and between canisters. The separation between canisters is 3 m for both the HLW and SF emplacement tunnels. In a separate sector of the repository, there are larger diameter emplacement tunnels for ILW. A cross-section of the ILW tunnels is shown in Fig. 3.

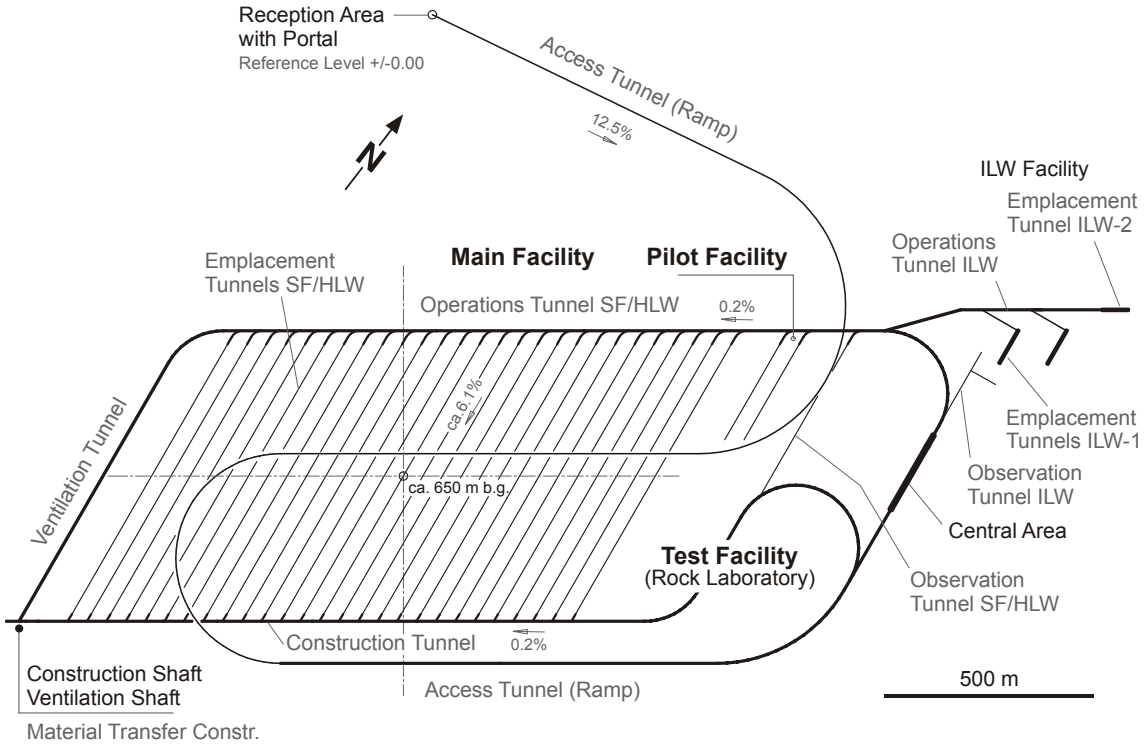

Fig. 1: Overall layout of the repository for spent fuel (SF), high-level waste (HLW) and intermediate level waste (ILW) in Opalinus Clay

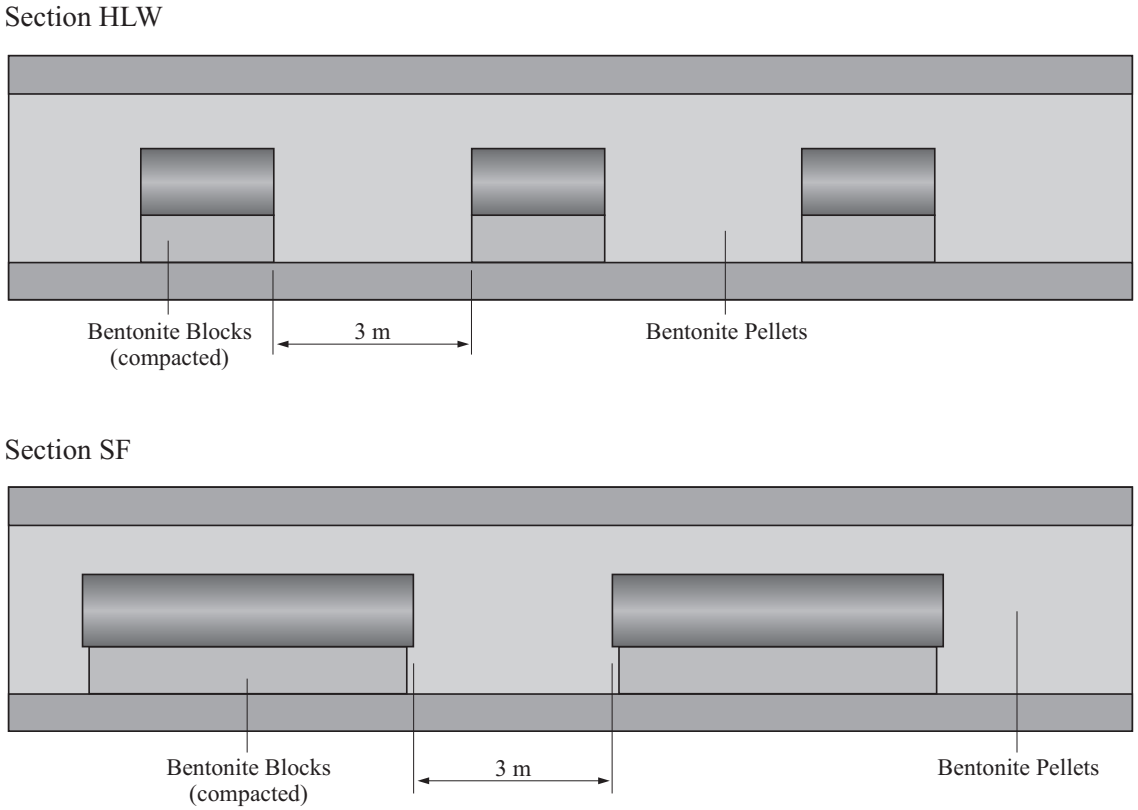

Fig. 2: Longitudinal section of emplacement tunnels for HLW and SF

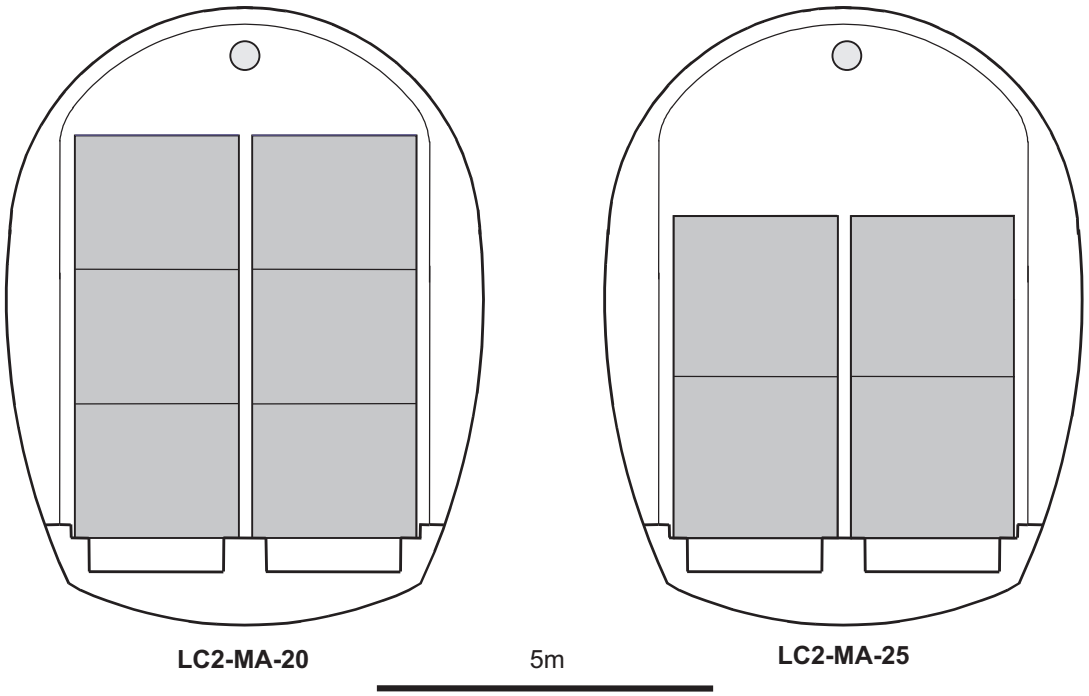

Fig. 3: Cross-section of the ILW emplacement tunnel

Canisters for HLW and Spent Fuel

The carbon steel HLW canisters, with a diameter of 0.94 m and a length of 2 m, are of the design assumed in Kristallin-I (NAGRA 1994) and are shown in Fig. 4. The total mass of steel and glass is 8.87 t The canister is represented in temperature calculations as a simple thick walled cylinder. For the SF canisters, mild steel is cast in the form of a cylinder with vacant channels that would contain either BWR or PWR fuel assemblies, as shown in Figs. 5 and 6. The canisters are 4.7 m long and have a diameter of 1.05 m. The internal canister geometry is complex and is simplified for the purposes of temperature calculations. Because there is no need to calculate internal canister temperatures, the canister is represented as a thick walled cylinder, with a total mass (including fuel) of 26.2 t, with a single central void space.

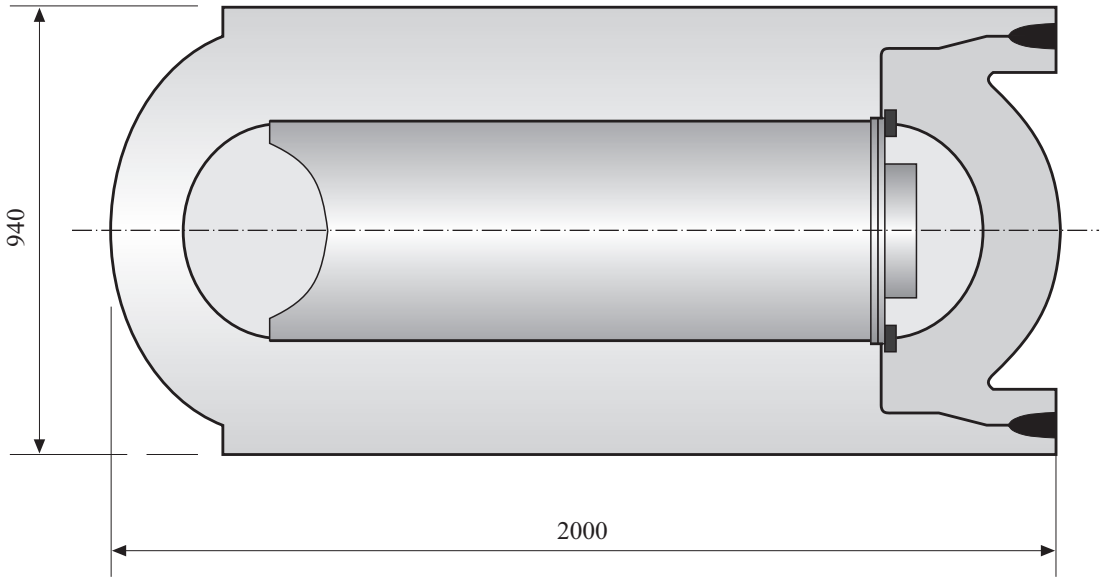

Fig. 4 Canister for HLW

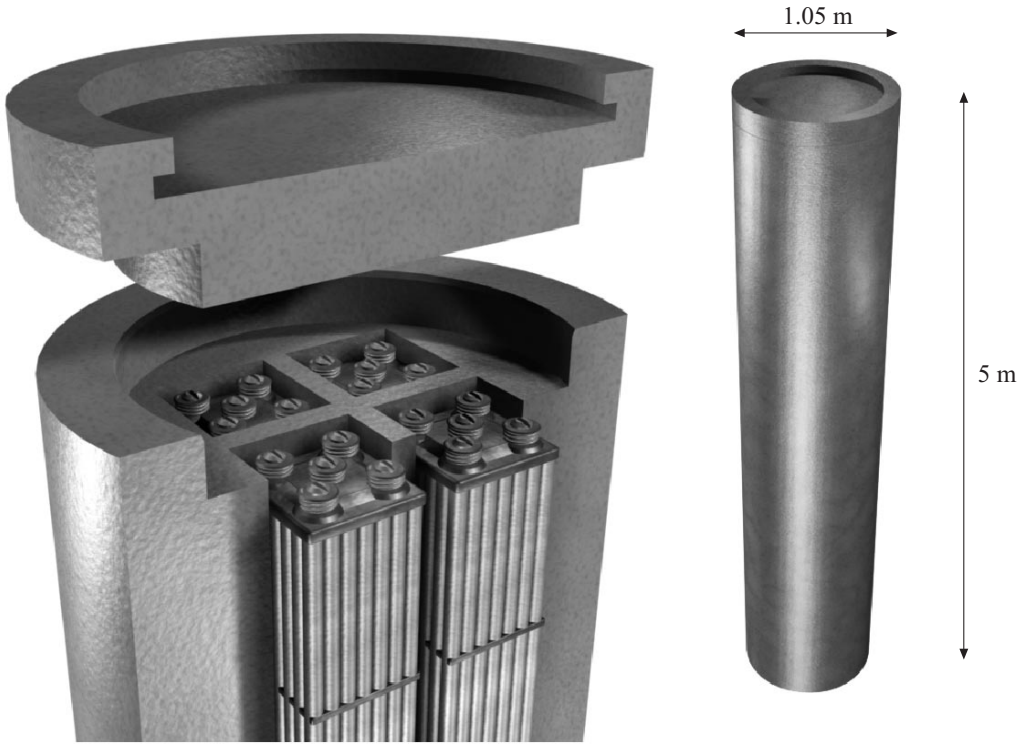

Fig. 5: Canister for PWR SF

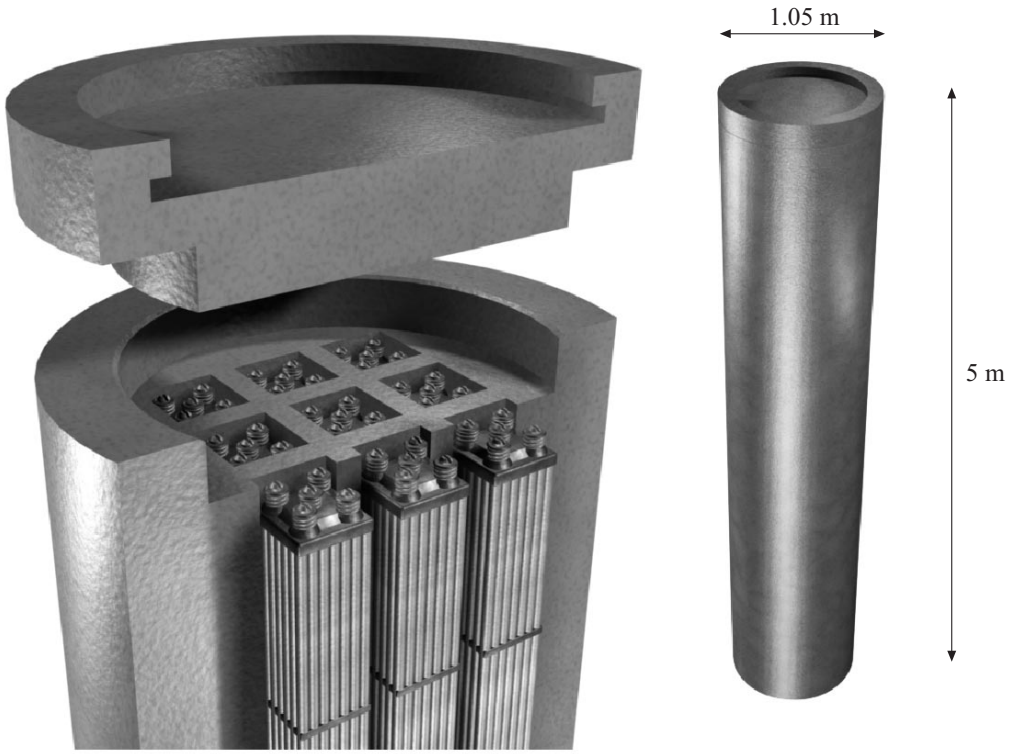

Fig. 6: Canister for BWR SF

5 Thermal Properties of Wastes, Engineered Barrier System and Opalinus Clay

Thermal Output of Wastes

HLW Canisters

The present study considers the case of BNFL HLW glass canisters cooled for 40 years, for which the thermal output is given in Table 1 (MCGINNES 2002). No calculations have been performed for the case of COGEMA canisters, which have a lower decay heat of 538 W, as compared to 688 W for BNFL canisters. The data in Table 1 is for the reference average BNFL glass composition reported by MCGINNES (2002).

Table 1: Decay heat of BNFL HLW canister with a cooling time of 40 years (average composition) (MCGINNES 2002)

Time from repository closure (a)	0	3	10	30	100	300	1000	3000
Heat Output (W)	688	646	560	380	137	60	19.9	1.7
Time from repository closure (a)	1×10^4	3×10^4	1×10^5	3×10^5	1×10^6	3×10^6	1×10^7	
Heat Output (W)	0.64	0.3	0.17	0.23	0.23	0.12	0.01	

SF Canisters

The canister designs for SF, shown in Figs 5 and 6, are for either 9 boiling water reactor (BWR) or 4 pressurised water reactor (PWR) assemblies. The SF includes both UO_2 and MOX assemblies with a range of burn-ups and reactor discharge dates. MCGINNES (2002) performed a comprehensive evaluation of the characteristics of spent fuel assemblies discharged from the various Swiss power reactors. The calculations illustrated that, with the mixing of UO_2 fuel assemblies of different burn-ups within canisters, a heat output constraint of 1500 W after 40 years decay will be achievable for both BWR and PWR fuel canisters, provided the average burnup is 48 GWd/tIHM. For the case of PWR MOX fuel, the combination of 1 MOX assembly with 3 UO_2 assemblies, all with a reference average burnup of 48 GWd/tIHM, would typically lead to a heat output of ~1800 W after 40 years of decay, with the decay heat decreasing to less than 1500 W after about 55 years. For such a fuel combination with a cooling time shorter than 55 years, it is possible to meet the 1500 W constraint by reducing the fuel loading in a canister, as noted in Section 3.

MCGINNES (2002) recommended two cases that are representative of the canisters that would contain SF. These cases are referred to here as UO_2 canisters, designating canisters containing only UO_2 fuel assemblies (9 BWR or 4 PWR), or MOX/UO_2, canisters, which contain 1 PWR MOX assembly plus 3 PWR UO_2 fuel assemblies. The decay heat as a function of time for the BWR UO_2 canister with an average burnup of 48 GWd/tIHM is given in Table 2 (MCGINNES 2002). Because PWR fuel has the same average burnup and because the two canister types contain essentially the same fuel mass, calculations for the canister thermal data given in Table

2 are considered representative for all canisters containing only UO_2 fuel. The slight difference between the values given by MCGINNES (2002) and the values in Table 2 result from the use of different fuel depletion codes and are too small to affect the temperature calculations.

Table 2: Decay heat of a UO_2 canister containing 9 BWR UO_2 assemblies (40 years interim storage) with an average burnup of 48 GWd/tIHM (MCGINNES 2002)

Time from repository closure (a)	0	3	10	30	100	300	1000	3000
Heat Output (W)	1490	1420	1280	976	522	284	120	47
Time from repository closure (a)	1×10^4	3×10^4	1×10^5	3×10^5	1×10^6	3×10^6	1×10^7	
Heat Output (W)	28	11	2.4	1.4	0.87	0.49	0.21	

For the MOX/UO_2 canister, containing PWR fuel (1 MOX and 3 UO_2 assemblies), the time-dependent decay heat is given in Table 3. Temperature calculations are based on storage times prior to emplacement in the repository of 40 years for UO_2 canisters and 55 years for MOX/UO_2 canisters.

Table 3: Decay heat of MOX/UO_2 canister, containing 3 PWR UO_2 assemblies and 1 PWR MOX assembly (55 years interim storage), all with a burnup of 48 GWd/tIHM (MCGINNES 2002)

Time from repository closure (a)	0	3	10	30	100	300	1000	3000
Heat Output (W)	1500	1450	1330	1080	696	422	177	68
Time from repository closure (a)	1×10^4	3×10^4	1×10^5	3×10^5	1×10^6	3×10^6	1×10^7	
Heat Output (W)	39	14	3.0	1.8	1.1	0.59	0.21	

Thermal Properties of the EBS and Opalinus Clay

Thermal Properties of Canisters and Bentonite

The thermal conductivities and heat capacities of steel and bentonite are given in Table 4**.** Values for steel are taken from SATO et al. (1998). The initial temperature of the spent fuel canister surface is calculated to be ~60°C prior to emplacement of bentonite, assuming radiative heat transfer to air in the emplacement tunnel and a constant air temperature of 38°C (see Appendix A).

Table 4: Thermal properties of steel, bentonite, Opalinus Clay and adjacent formations used in the finite-element calculations

Material	Thermal conductivity ($W\ m^{-1}\ K^{-1}$)	Heat Capacity ($MJ\ m^{-3}\ K^{-1}$)	Initial temperature (^0C)
steel	52	3.05	60
bentonite (2% moisture)	0.4	1.2	38
bentonite (saturated)	1.35	2.4	38
Opalinus Clay EDZ (0.5 m thick)	1.5	2.3	38
Upper Opalinus Clay and upper confining units (550 to 670 m)	3.2 (horizontal) 1.8 (vertical)	2.3	As defined by the thermal gradient (see Fig. 7)
Lower Opalinus Clay and lower confining units (670 to 750 m)	2.0 (horizontal) 1.3 (vertical)	2.3	As defined by the thermal gradient (see Fig. 7)
Overlying and underlying formations	3.2	2.3	As defined by the thermal gradient (see Fig. 7)

It is expected that the granular bentonite will have an initial moisture content of 2 % at emplacement (NAUNDORF & WOLLENBERG 1992). The thermal conductivity of bentonite is strongly dependent on moisture content, which is expected to remain low for a considerable time after backfilling of the tunnels because of the low hydraulic conductivity of Opalinus Clay ($<10^{-13}$ m s^{-1}). A thermal conductivity of 0.4 W m^{-1} K^{-1} for low moisture content bentonite was selected based on a value of 0.39 W m^{-1} K^{-1} reported by GRAY (1993) for dry compacted blocks of bentonite, the value of 0.5 W m^{-1} K^{-1} given in NAGRA (1985) for bentonite blocks with a 2% moisture content, and the value of ~0.4 W m^{-1} K^{-1} reported by VOLCKAERT et al. (1996) for dry granular Boom clay backfill at Mol (BACCHUS 2 test). For the heat capacity of dry bentonite, a value of 1.2 MJ m^{-3} K^{-1} is selected, based on values of ~1.8 MJ m^{-3} K^{-1} **(**HOPKIRK & WAGNER 1985) for compacted bentonite with a 2% water content, 1.14 MJ m^{-3} K^{-1} (PNC 1992), for dry compacted bentonite and 1.2 MJ m^{-3} K^{-1} (GRAY 1993) for dry bentonite.

The impact of increased moisture content on temperatures is evaluated by considering the additional case of saturated bentonite. A thermal conductivity of 1.35 W m^{-1} K^{-1} is selected for this case, based on the review and measurements of BÖRGESSON et al. (1994). This value agrees well with the values of 1.4 W m^{-1} K^{-1} (GRAY 1993), 1.7 W m^{-1} K^{-1} (PNC 1992), and

results from in situ thermal conductivity measurements on granular bentonite in the BACCHUS test reported by VOLCKAERT et al. (1996), which ranged from 1.4 to 2.5 W m^{-1} K^{-1}.

For heat capacity, PNC (1992) adopts a value of 2.1 MJ m^{-3} K^{-1}, whereas GRAY (1993) gives a value of 2.4 MJ m^{-3} K^{-1} for saturated bentonite powder, which is adopted here.

Thermal Properties of Opalinus Clay

Far-field temperature initial and boundary conditions are required for the temperature calculations. These are reported in NAGRA (2001). A value of 3.2 W m^{-1} K^{-1} is adopted for the thermal conductivity of sedimentary sequences overlying and underlying the Opalinus Clay, based on measurements that range from 2.5 to 3.6 W m^{-1} K^{-1}, reported in NAGRA (2001). Measurements in the Benken borehole permit calculation of the thermal conductivity and heat capacity of Opalinus clay (NAGRA 2001). The upper Opalinus Clay at Benken (558-625 m) plus overlying clay-rich sediments (500-558 m) have a higher quartz content and thus a higher thermal conductivity (see Fig. 7). The lower Opalinus clay at Benken (625-650 m) and underlying sediments (650-700 m) have a lower quartz content and thus a lower thermal conductivity. The presence of bedding planes results in a higher thermal conductivity in the horizontal plane than in the vertical plane (Table 4).

The correctness of the thermal conductivity values for Opalinus Clay and overlying and underlying formations given in Table 4 can be assessed by using the data in a simple heat conduction model to calculate the temperature profile in the Benken borehole. The results of such a calculation are shown in Fig. 7, in which it is seen that agreement between the calculated profile and the measured profile is excellent.

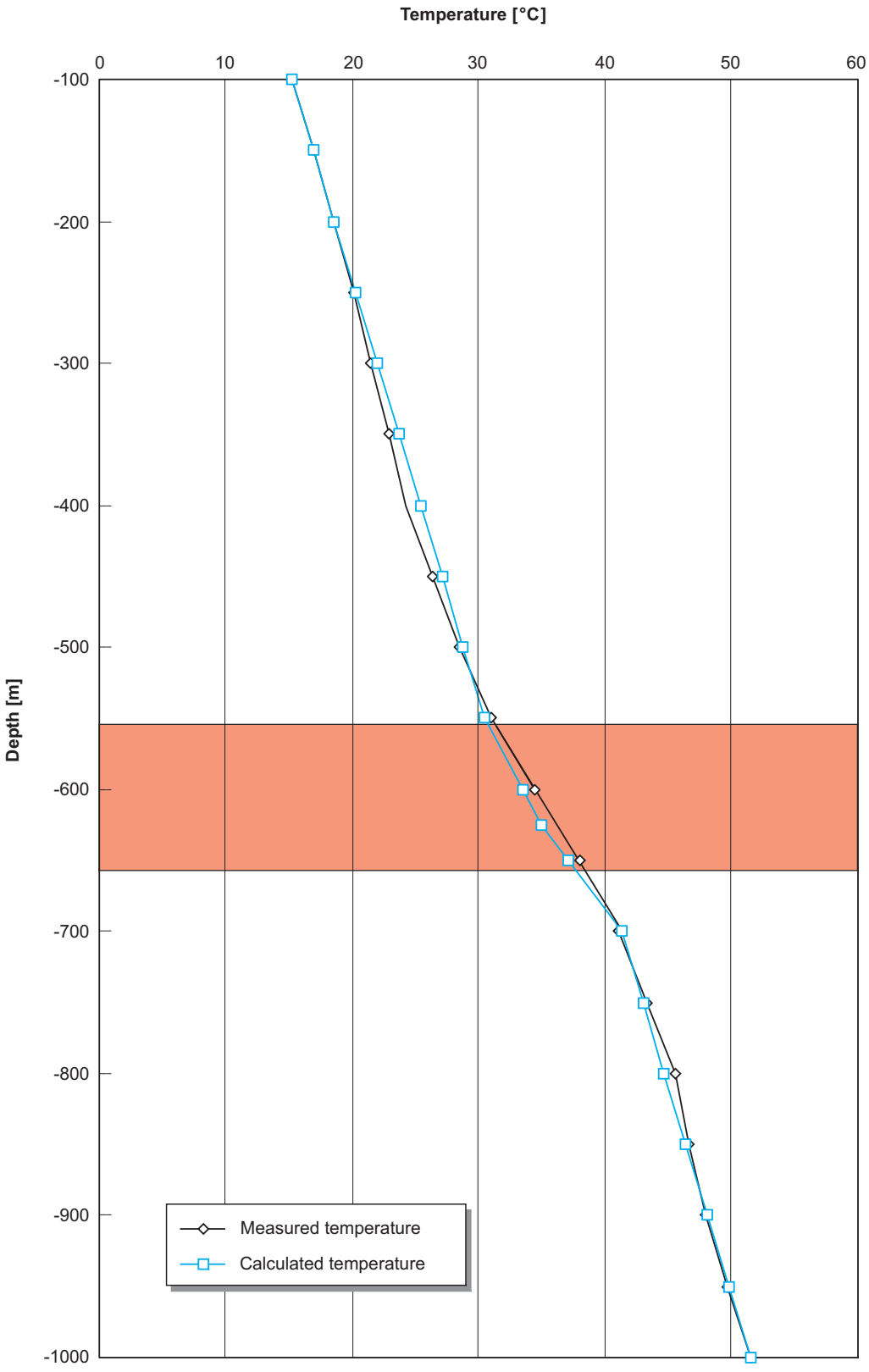

Fig. 7: Comparison of the measured temperature profile in the Benken borehole with the profile calculated using a heat conduction model and the data in Table 4: The host rock is indicated by the shaded area.

The excavation-disturbed zone (estimated to be 0.5 m thick) of a SF/HLW emplacement room in the repository may have a reduced water content as result of ventilation, which would decrease the thermal conductivity slightly, thus a reduced value is estimated for the EDZ.

Fig. 8 shows the correspondence between the intervals at Benken and their thermal conductivities and the intervals assumed for the thermal model. The difference in elevations arises because the hypothetical repository is located some distance from the Benken borehole.

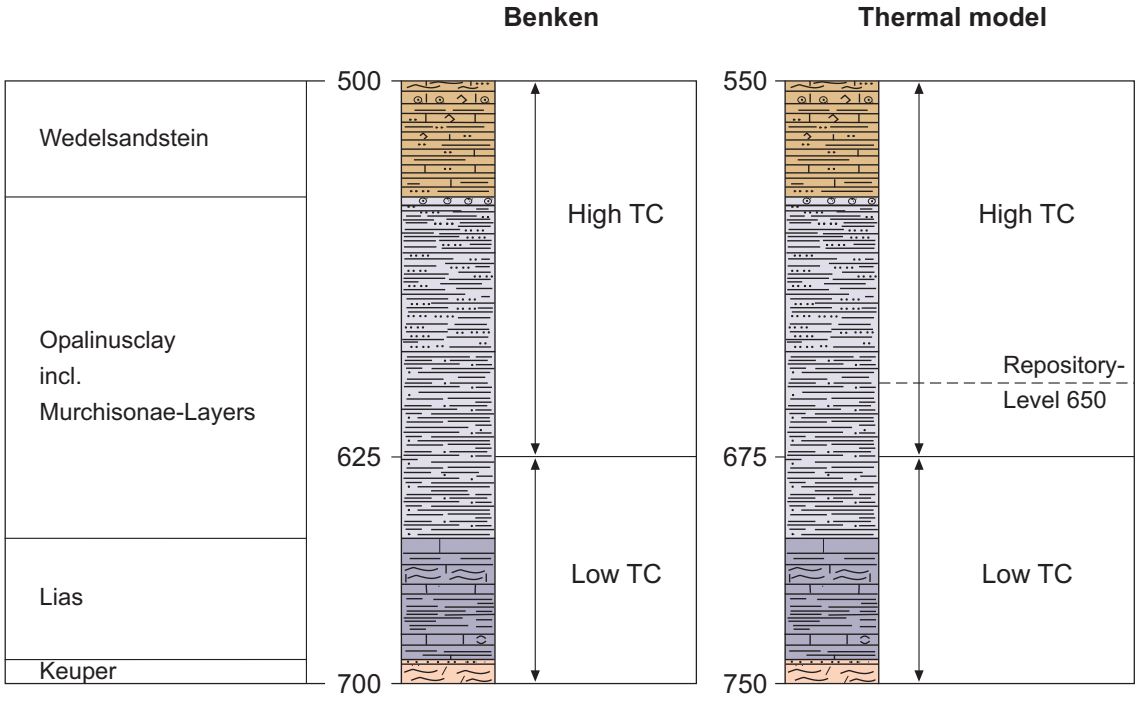

Fig. 8: Correspondence between the Benken elevations and thermal conductivities from NAGRA (2001) and the model elevations for the Opalinus Clay repository. High TC refers to higher thermal conductivity (high quartz content) Opalinus clay and overlying sediments; Low TC refers to low thermal conductivity Opalinus Clay and underlying sediments (see Table 4). The dashed line in the thermal model domain is the centre of the Opalinus clay.

6 Finite-Element Modelling of Temperature Evolution of the SF/HLW Emplacement Tunnels

The three-dimensional equations describing temperature evolution are solved using COLENCO's CGM-code with an iterative solver and preconditioning (GENTER &. SCHINDLER, 1996). Heat transport is assumed to occur entirely by conduction. The contribution from convection is expected to be negligible, because of the low gas and hydraulic permeabilities of bentonite and Opalinus Clay. This is confirmed by calculations given in Appendix B.

The geometry of the analysis domain is illustrated in Fig. 9. The vertical sides of the domain are assumed to be zero-flux boundaries (symmetry planes). At the upper and lower boundaries, a constant temperature is imposed. These boundaries are far away from the heat source and calculations confirm the validity of the assumption. Temperatures are plotted at the indicated points in both the vertical and horizontal planes.

The three-dimensional finite-element mesh is shown in Fig. 10. It contains about 9000 8-noded elements. The mesh is refined in the area of interest, i.e. in the vicinity of the heat source, and is more coarse towards the boundaries, the biggest element being located at the upper and lower extremities of the mesh. The generation algorithm guarantees optimum numerical performance by controlling minimal angles and aspect ratios (RUPPERT 1995, SHEWCHUK 1997). The unstructured generation allows for a very high-quality mesh with a minimum number of elements. Test calculations of grid convergence with meshes of different size confirm the suitability of the discretisation.

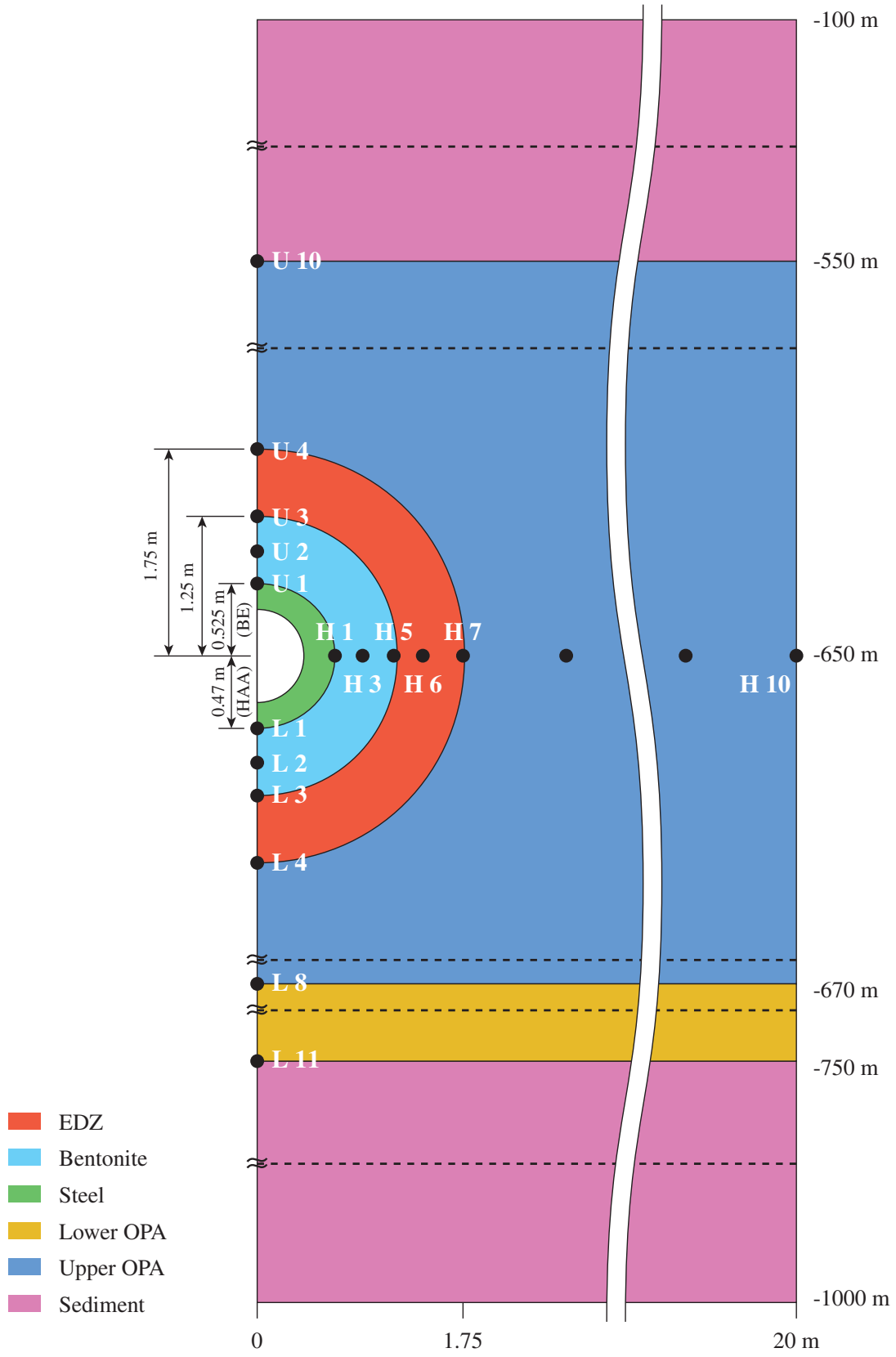

Fig. 9: Vertical section of the analysis domain, showing the locations at which the temperatures are calculated. Note that the terms upper OPA and lower OPA refer to domains that include additional overlying and underlying sediments.

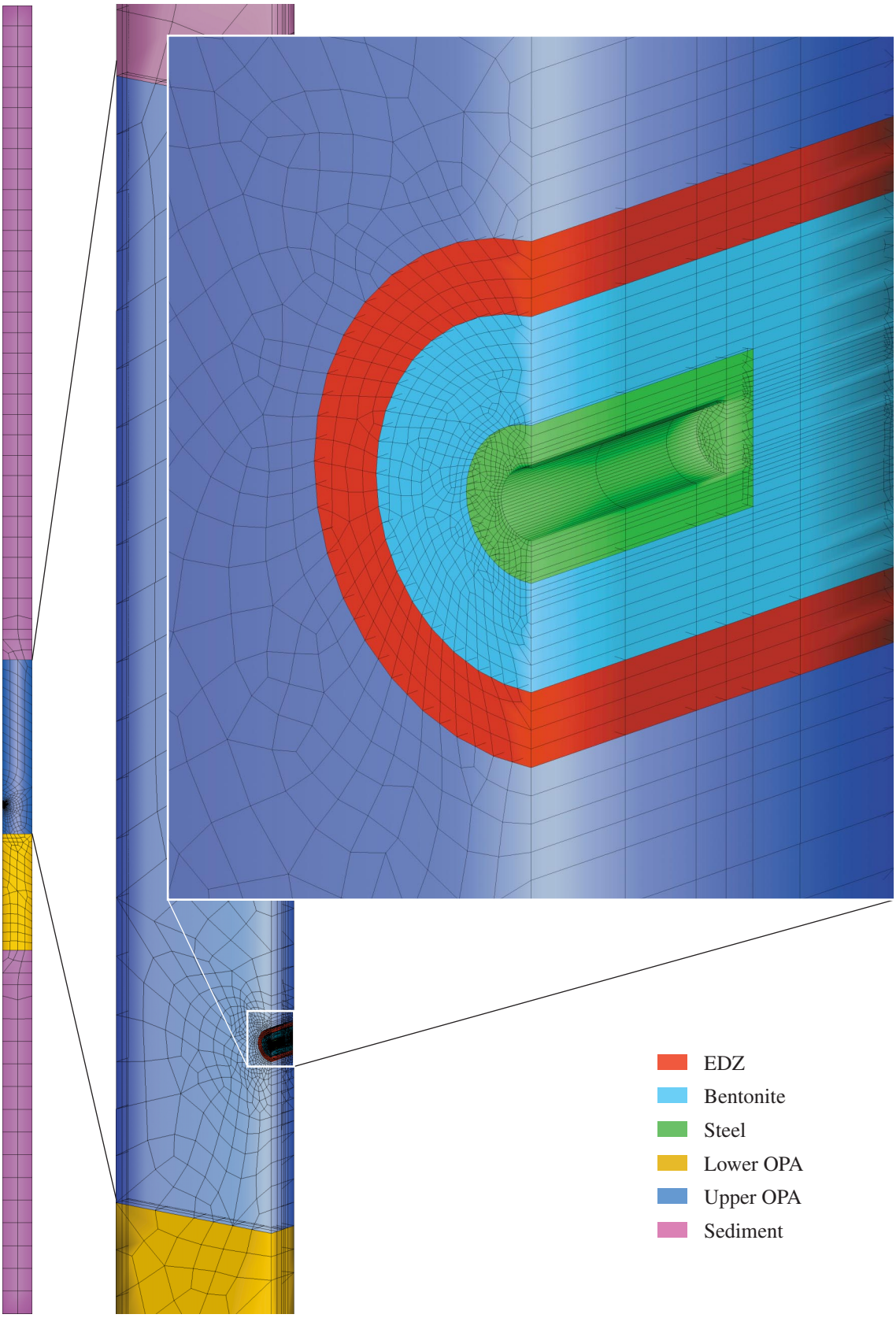

Fig. 10: Three-dimensional finite-element mesh for the temperature evolution calculations for spent fuel canisters

7 Results of Temperature Evolution Calculations

Temperature Distributions for HLW Emplacement Tunnels

The time-dependent temperature distribution in the horizontal orientation for HLW emplacement tunnels is shown in Fig. 11 for low thermal conductivity bentonite. The results show that, for the expected condition of low moisture content bentonite, the peak temperature of ~150°C at the canister/bentonite interface (H1) is reached within a few years. Within 100 years, the temperature decreases to ~80°C. The temperature at the mid-bentonite position (H3) remains below 100°C. Temperatures within the Opalinus Clay (H7 and H10) never exceed 70°C. The temperature distributions after 26 years, the time at which the temperature in the outer bentonite reaches a maximum, are shown in Fig. 12. For the hypothetical case of bentonite saturated from the beginning, temperatures are well below 100°C on the canister surface and throughout the bentonite, as shown in Fig. 13.

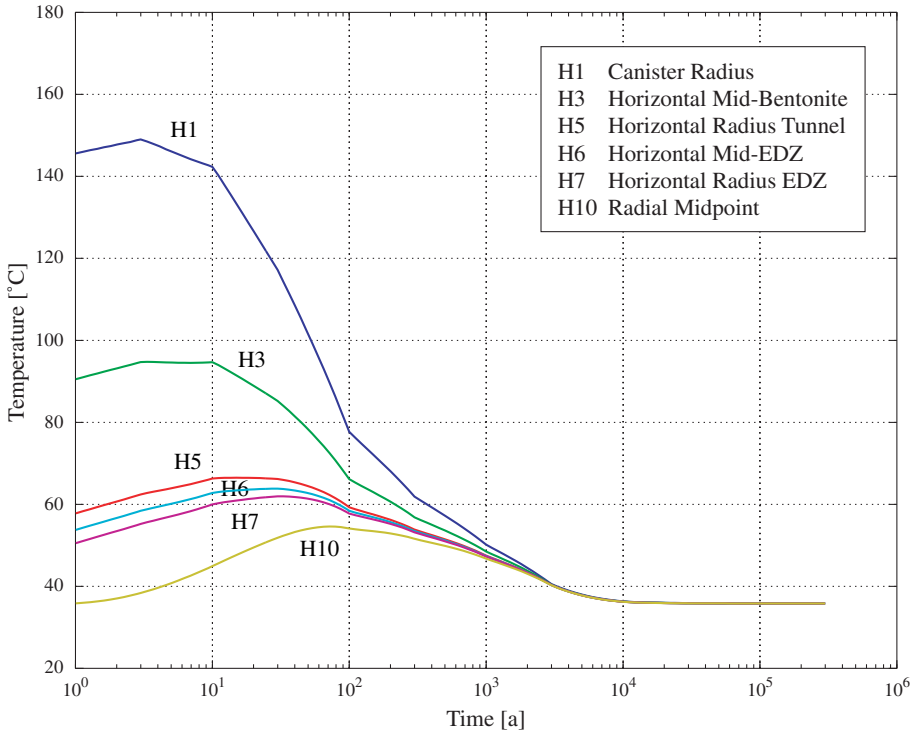

Fig. 11: The time-dependent temperature distribution in the horizontal orientation for emplacement tunnels for HLW canisters for the case of low bentonite thermal conductivity (low moisture content)

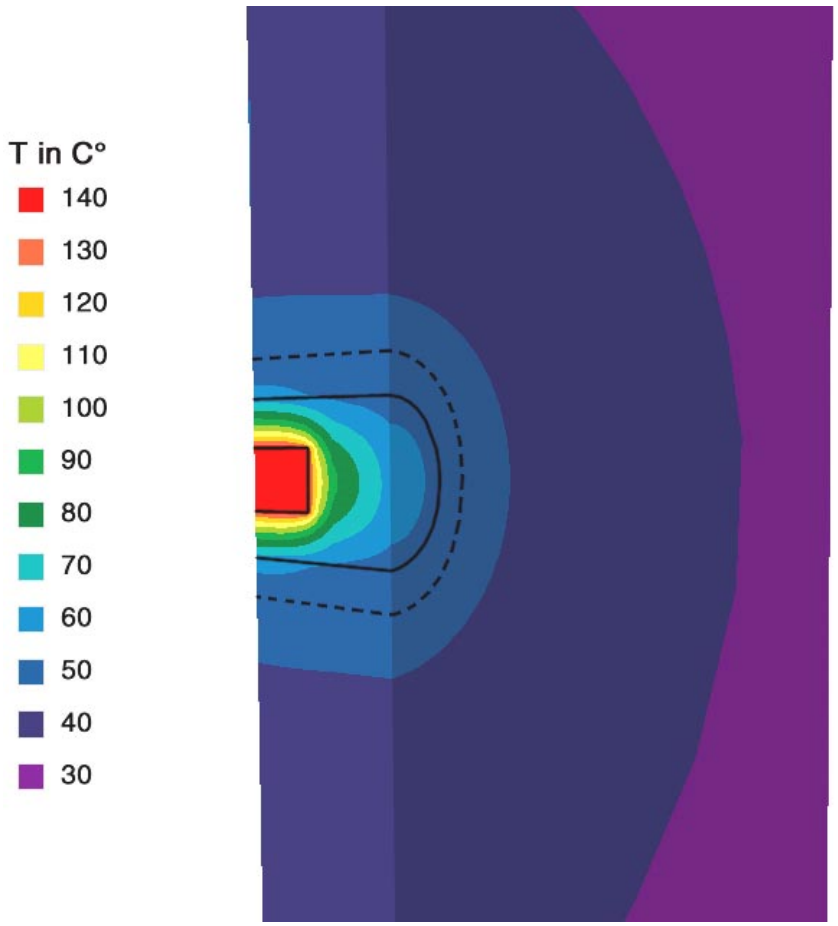

Fig. 12: Temperature profiles 26 years after emplacement, for a disposal tunnel with canisters containing HLW, for a low bentonite thermal conductivity (low moisture content). The canister is represented by the rectangle at the centre of the tunnel and the solid and dashed lines represent the tunnel boundary (R = 1.25 m) and the assumed outer boundary of the EDZ (R = 1.75 m), respectively. The time of 26 years represents the time of maximum temperature of the outer part of the bentonite. The vertical cross-sections are at mid-tunnel and midway between canisters.

.

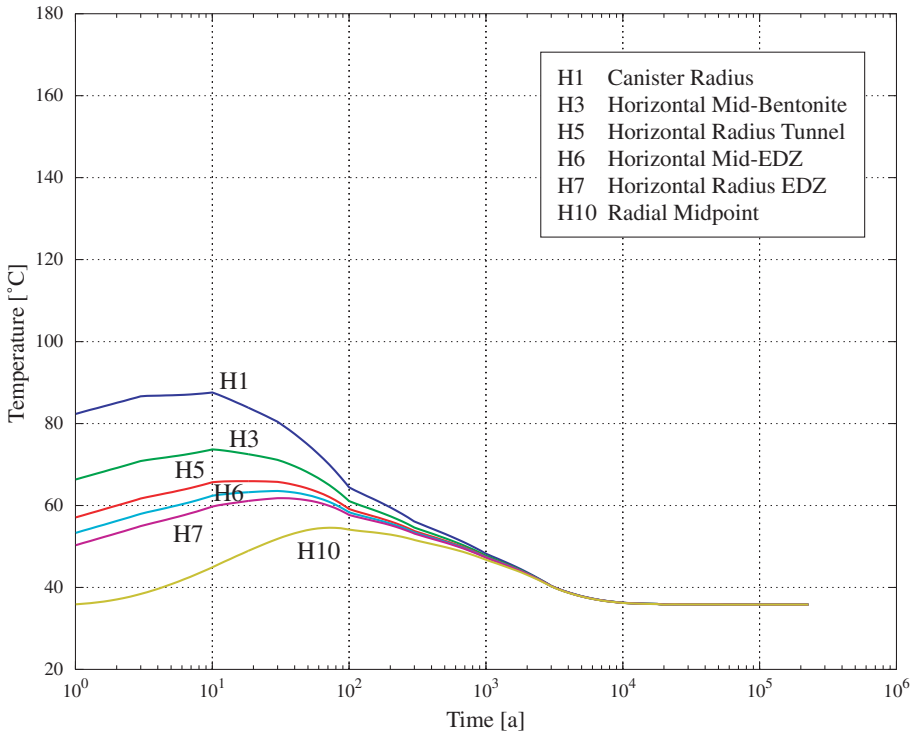

Fig. 13: The time-dependent temperature distribution in the horizontal orientation for emplacement tunnels for HLW canisters for the case of high bentonite thermal conductivity (high moisture content)

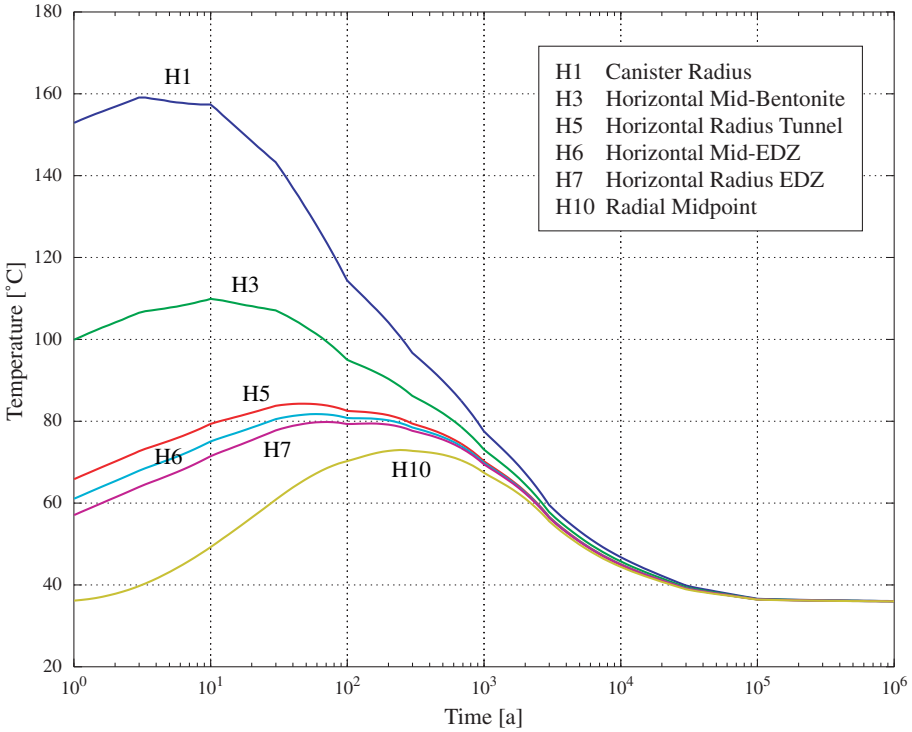

Fig. 14: The time-dependent temperature distribution in the horizontal orientation for emplacement tunnels for UO_2 fuel canisters for the case of low bentonite thermal conductivity (low moisture content)

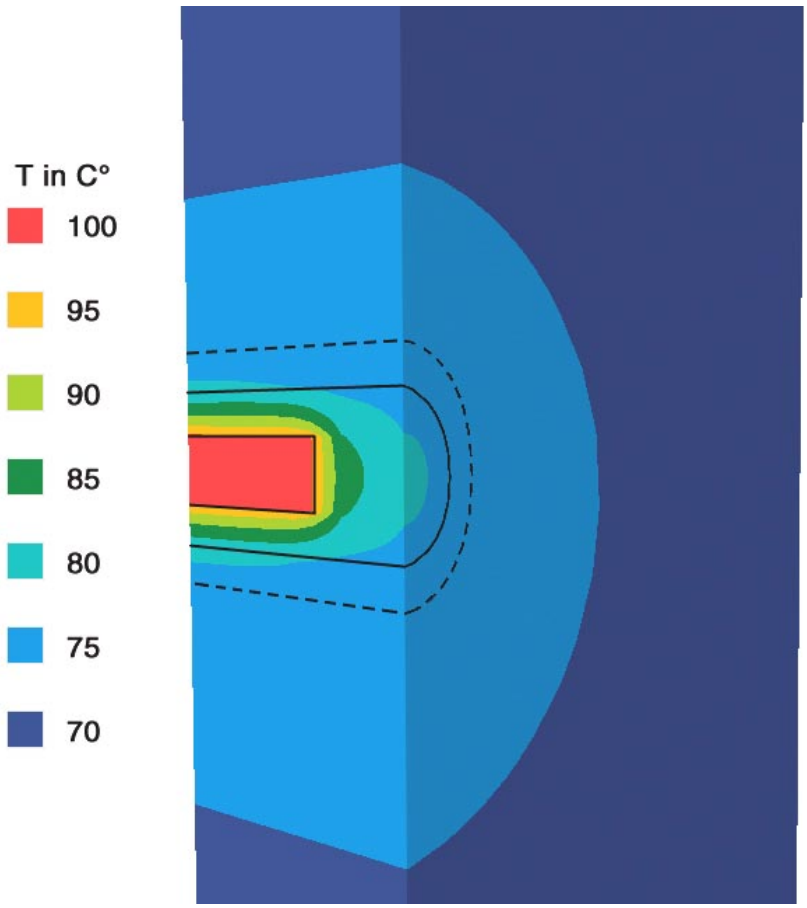

Fig. 15: Temperature profiles 244 years after emplacement, for a disposal tunnel with canisters containing UO_2 fuel, for a low bentonite thermal conductivity (low moisture content). The canister is represented by the rectangle at the centre of the tunnel and the solid and dashed lines represent the tunnel boundary (R = 1.25 m) and the assumed outer boundary of the EDZ (R = 1.75 m), respectively. The time of 244 years represents the time of maximum temperature of the bentonite region between canisters. The vertical cross-sections are at mid-tunnel and midway between canisters.

Temperature distributions in the vertical orientation, as well as cross-sections illustrating temperature distributions at other times, are given in Appendix C.

Temperature Distributions for SF Emplacement Tunnels

The time-dependent temperature distributions for UO_2 canisters are shown in Fig. 14 for the case of low thermal conductivity bentonite. For the expected initially dry conditions in the bentonite, the peak temperature at the canister/bentonite interface (H1) reaches ~160°C. Within 1000 years, the temperature decreases to ~80°C (cf. 100 years for HLW glass). The temperature at the mid-bentonite position (H3) reaches almost 110°C. At the axial mid-point between canisters, the temperature reaches a maximum of ~85°C, as shown in Fig. 15. Temperatures within the Opalinus Clay remain below ~90°C and within several hundred years, have reached a maximum of ~75°C about 7 m from the tunnel boundary. For saturated bentonite, the peak temperature at the canister/bentonite interface (H1) is 100°C, as shown in Fig. 16. The temperatures within the bentonite remains in the 80 to 90°C range for several hundred years.

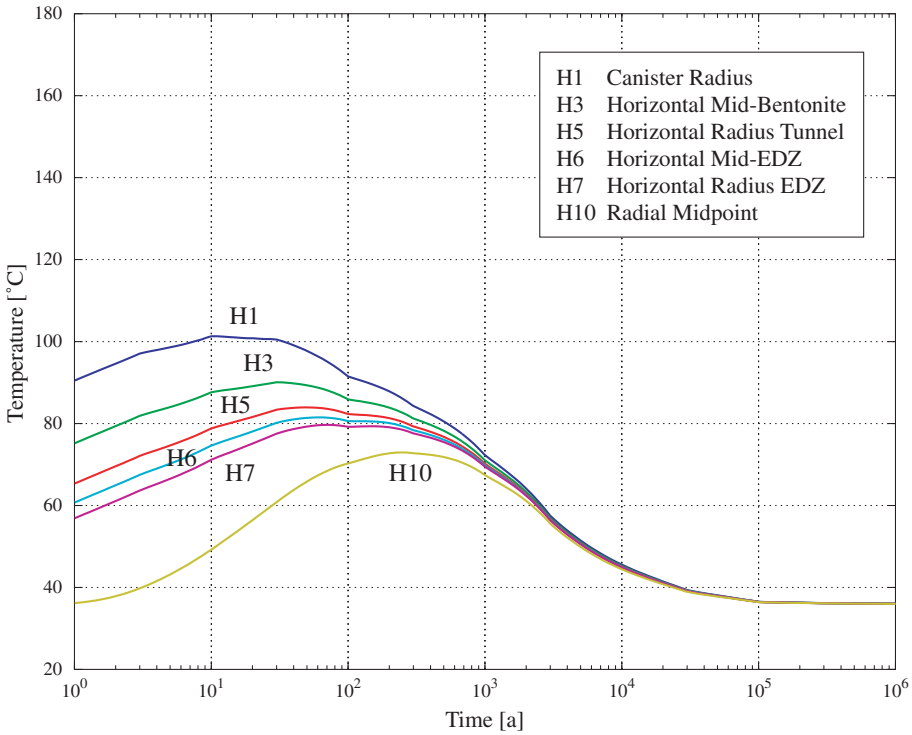

Fig. 16: The time-dependent temperature distribution in the horizontal orientation for emplacement tunnels for UO_2 fuel canisters for the case of high bentonite thermal conductivity (high moisture content)

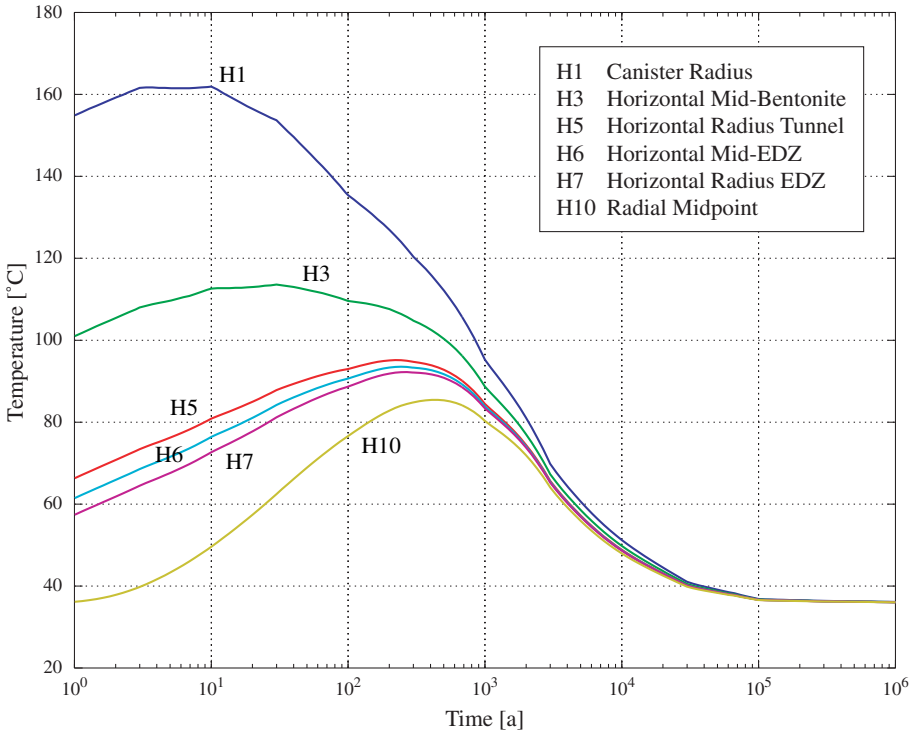

Fig. 17: The time-dependent temperature distribution in the horizontal orientation for emplacement tunnels for MOX/UO_2 fuel canisters for the case of low bentonite thermal conductivity (low moisture content)

For the case of MOX/UO_2 canisters, the results for dry conditions are shown in Fig. 17. The increased heat output relative to UO_2 canisters in the time frame of 30 to 1000 years (cf. Tables 2 and 3) leads to a significant extension of the time over which the bentonite/canister interface is above 100°C. The temperature of the mid-bentonite position remains over 100°C for ~500 years. At the axial mid-point between canisters, the temperature reaches a maximum of ~95°C after about 250 years, as shown in Fig.18. For saturated bentonite, the peak temperature at the canister/bentonite interface (H1) is below 110°C, as shown in Fig. 19. The present results confirm the previous limited calculations for Opalinus Clay presented in SATO et al. (1998). In that report, the temperature at the mid-bentonite position for a canister with a 1500 W initial heat output for saturated conditions was calculated to peak at ~95°C, for an assumed ambient temperature of 35°C. The present study calculates a peak temperature of ~100°C for the case of saturated bentonite for the measured ambient temperature at 650 m depth of 38°C.

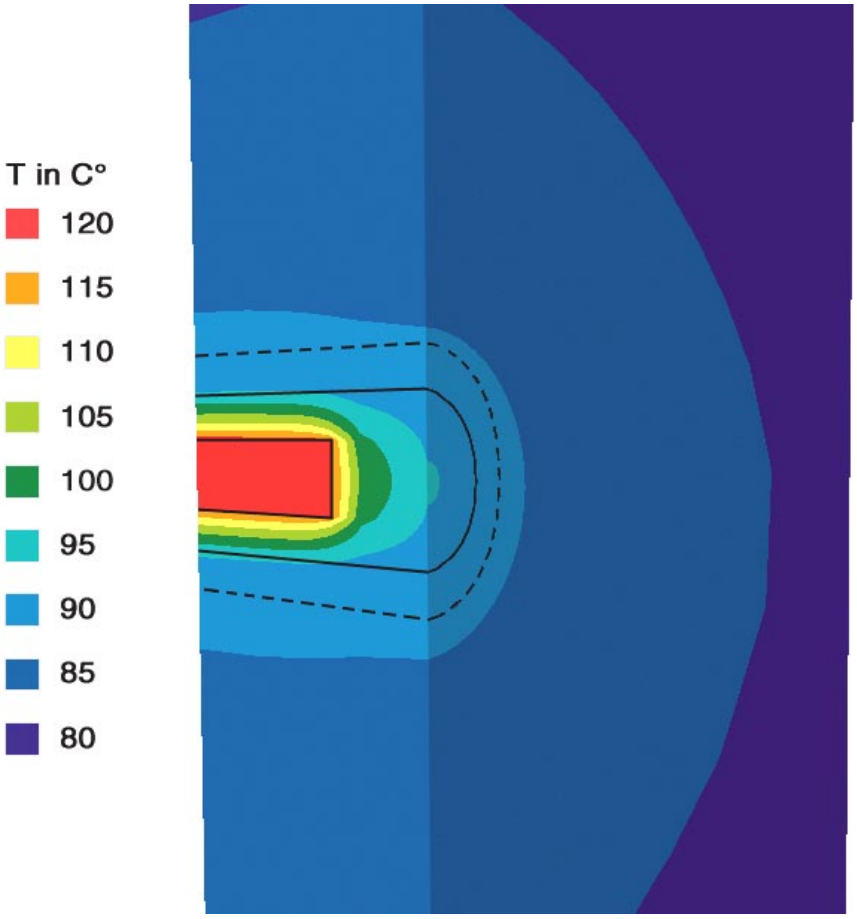

Fig.18: Temperature profiles for a disposal tunnel with canisters containing MOX/UO_2 fuel canisters 268 years after emplacement, for a low bentonite thermal conductivity (low loisture content). The canister is represented by the rectangle at the centre of the tunnel and the solid and dashed lines represent the tunnel boundary (R = 1.25 m) and the assumed outer boundary of the EDZ (R = 1.75 m), respectively. The time of 268 years represents the time of maximum temperature of the bentonite region between canisters. The vertical cross-sections are at mid-tunnel and midway between canisters.

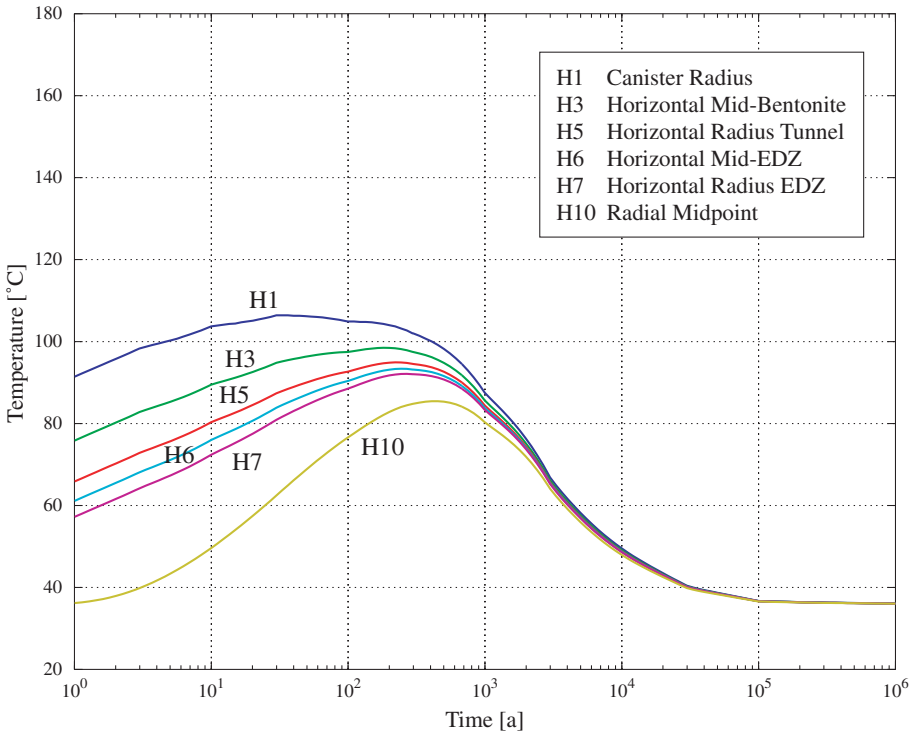

Fig. 19: The time-dependent temperature distribution in the horizontal orientation for emplacement tunnels for MOX/UO_2 fuel canisters for the case of high bentonite thermal conductivity (high moisture content).

Temperature distributions in the vertical orientation and for various times are given in Appendix C**.** Of interest is the maximum temperature reached at the upper boundary of the Opalinus Clay and overlying sediments, ~100 m above the repository. The peak temperature of 55-60°C at this elevation is reached after about 1000 years (Fig. App. C-10), for the case of MOX/UO_2 canisters.

Temperature Distributions for ILW Emplacement Tunnels

As noted in Section 1, calculations of the temperature evolution in ILW emplacement tunnels have also been performed (Appendix D). Heat is produced as a result of cement hydration and from decay of the wastes, with the former source providing the largest contribution. Temperatures reach ~50°C within the tunnels, decreasing to ambient temperature (38°C) within a few thousand years.

8 Assessment of the Accuracy of the Temperature Evolution Calculations

It is generally considered that the modelling of temperatures around repositories is more reliable and robust than is the modelling of other processes (e.g. hydro-mechanical and hydrogeological processes) (GOBLET & DE MARSILY 2000). Nonetheless, some testing of the reasonableness and correctness of the results obtained is clearly desirable. This was done using an analytical benchmark. In this calculation, the temperature as a function of time was calculated at a distance of 100 m above the plane of the emplacement tunnels. The details of the analysis are given in Appendix E. The results, shown in Fig. 20, indicate excellent agreement between the analytical and numerical models.

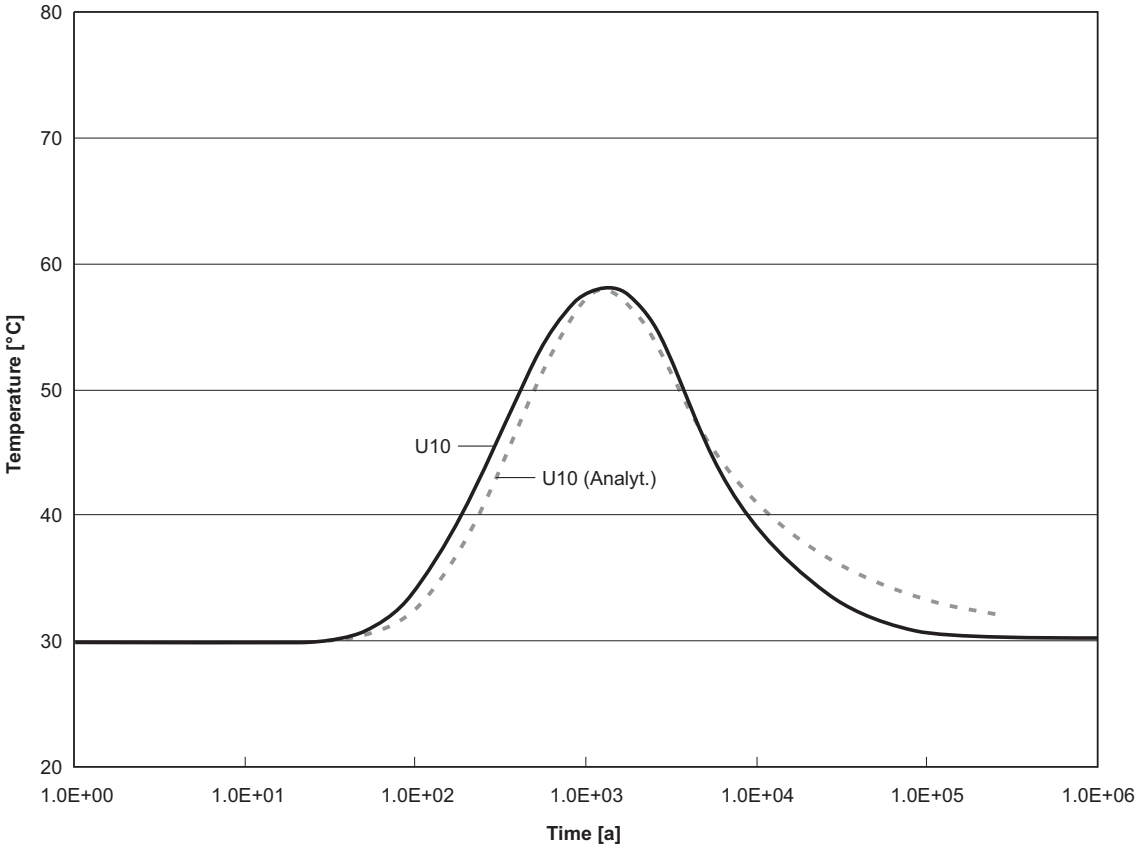

Fig. 20: Temperature-time plot for a location 100 m above the emplacement tunnels containing MOX/UO_2 fuel canisters (U10). The curve for the U10 position is from Fig. C-10. The calculation method is discussed in Appendix E.

9 Conclusions

The results of temperature calculations for SF and HLW emplacement tunnels in the present report illustrate clearly the significance of low bentonite thermal conductivity and the low permeability of Opalinus Clay in determining temperatures at the canister surface and in the bentonite backfill. These two characteristics are considered desirable with regard to delaying access of water to the canister and the waste. The temperature is expected to reach ~160°C at the surface of spent fuel canisters and ~150°C at the surface of HLW canisters. Because of the low permeability of Opalinus Clay, it is considered extremely unlikely that the temperatures calculated for saturated conditions will actually be realised. The calculations confirm the importance of understanding the effects of elevated temperatures on bentonite performance.

Given the experience with finite-element calculations in previous studies (SATO et al. 1998) and the analytical confirmation of the far-field temperature discussed in Appendix E, there is high confidence in the projected temperature-time evolution of the repository.

Calculations of the temperature in ILW tunnels indicate that temperatures will peak at no more than ~50°C.

10 Acknowledgements

The authors thank Lars Ageskog of SWECO for his comments and suggestions on a draft version of this report.

11 References

BÖRGESSON, L., FREDRIKSON, A. & JOHANNESON, L-E. (1994): Heat conductivity of buffer materials. SKB Technical Report 94-29.

COUTURE, R. (1985): Steam rapidly reduces the swelling capacity of bentonite. Nature 318, p.50.

GENTER, M. & SCHINDLER, M. (1996): Das Programm CGM, Colenco – Bericht 4073 / 4, Januar 1996, Baden, Schweiz

GOBLET, P. & DE MARSILY, G. (2000): Evaluation of the thermal effect in a KBS-3 type repository, SKI Report 00:18, SKI, Stockholm.

GRAY, M.N. (1993): OECD/NEA International Stripa Project, Overview Volume III. Engineered barriers, SKB.

HOPKIRK, R.J. & WAGNER, W.H. (1985): Thermal loading in the near field of repositories for high and intermediate level waste, Nagra Technical Report 85-54.

JNC (2000): H12: Project to Establish the Scientific and Technical Basis for HLW Disposal in Japan, JNC/TN 1410, Tokyo, Japan.

LUTZE, W. (1988): Silicate glasses in Radioactive Waste Forms for the Future, W. Lutze and R.C. Ewing, Eds., Elsevier, Amsterdam, pp. 1-159.

MCGINNES, D. & SCHNEIDER, J.W. (1998): Packaging of high burn-up UO_2 and MOX spent fuel considering temperature restrictions in the near field of a repository. In Mat. Res. Soc. Symp. Proc. 506, pp. 927 - 928. MRS, Warrendale, Pennsylvania.

McGINNES; D. (2002): Model radioactive waste inventory for reprocessing waste and spent fuels. Nagra Technical Report NTB 01-01.

NAGRA (1985): Project Gewähr 1985. Nuclear waste management in Switzerland: Feasibility studies and safety analyses, Nagra Project Report NGB 85-09.

NAGRA (1994): Kristallin-1 Safety Assessment Report, Nagra Technical Report NTB 93-22.

NAGRA (2001): Sondierbohrung Benken Untersuchungsbericht, Nagra Technical Report NTB 00-01.

NAUNDORF, W. & WOLLENBERG, R. (1992): Herstellung von Bentonit-Granulat mit hoher Schüttdichte zur Bohrlochabdichtung, Nagra Technical Report NTB 92-06.

NOLD, A. (2000): The Swiss HLW/ILW repository in Opalinus Clay. Programme, layout and emplacement of spent fuel canisters. Proc. DISTEC 2000, Berlin.

OSCARSON, D.W. & DIXON, D.A.. (1990): Effect of heating unsaturated bentonite on the swelling and hydraulic properties of subsequently saturated clay. In Proceedings of the Annual Conference and 1st Biennial Environmental Speciality Conference of the Canadian Society of Civil Engineering, Hamilton, Ontario, Volume II-1, 312-323.

PNC (1992): Research and development on geological disposal of high-level radioactive waste. PNC Technical Report TN 93-059, Tokyo, Japan.

PUSCH, R. & MADSEN, F.T (1995): Aspects on the Illitization of the Kinnekulle bentonites, Clays and Clay Minerals, 43, pp. 261-270.

PUSCH, R. (2000): On the effect of hot water vapor on MX-80 clay, SKB Technical Report TR-00-16, SKB, Stockholm.

PUSCH, R., KARNLAND, O., LAJUDIE, A & ATABEK, R (1992): Hydrothermal field experiment simulating steel canister embedded in expansive clay - Physical behaviour of the clay. Mat. Res. Soc. Symp. Proc. Vol. 257, pp. 547-556.

PUSCH, R., L.H. JOHNSON & P. BLÜMLING. (2002): Performance of strongly compressed MX-80 pellets under repository-like conditions. Proc. of a Workshop on Clay Microstructure and its Importance to Soil Behavior. Lund, Oct. 15-17, 2002.

RAIKO, H. & SALO, J.P. (1996): Design report of the canister for nuclear fuel disposal. Posiva Report 96-13.

RENSTRÖM, P. (1997): Calculation of the fuel temperature in vacuous storage canisters made of copper with cast steel insert, SKB Projekt PM Inkapsling Report 97-3420-23, SKB, Stockholm.

RUPPERT J. (1995): A Delaunay Refinement Algorithm for Quality 2-Dimensional Mesh Generation. Journal of Algorithms, n°18(3), pp. 548-585.

SATO, R., SASAKI, T., ANDO, K., SMITH, P.A. & SCHNEIDER, J.W.. (1998): Calculation of the Temperature Evolution of a Repository for Spent Fuel in Crystalline and Sedimentary Rocks. Nagra Technical Report NTB 97-02.

SHEWCHUK, J.R. (1997): Delaunay Refinement Mesh Generation. Thèse de l'université Canergie Mellon, Pittsburg, 207 pages.

SKB (1999): Deep repository for spent nuclear fuel SR-97-Post-closure safety, Main Report Vol. 3, SKB Technical Report TR 99-06.

VOLCKAERT, G., BERNIER, F. & DARDAINE, M. (1996): Demonstration of the in situ application of an industrial clay-based backfill material. (BACCHUS 2). European Commission Report EUR 16860.

WERME, L. (1998): Design premises for canister for spent fuel. SKB Technical Report TR 98-08.

Appendix A

Appendix A: HLW/SF: Estimation of the canister surface temperature at the time of emplacement

1 Introduction

Preliminary calculations of the temperature evolution in the planned repository OPA/SF have been reported by SATO et al. (1998). This investigation was based on previous calculations of the initial surface temperature of HLW canisters presented by HOPKIRK & WAGNER (1985), lacking specific information for SF canisters. These authors concluded that the surface temperature of the HLW canisters rises to approximately 65°C, based on the assumption of natural convection induced cooling of the canisters in air, but neglecting radiation-induced heat transfer (CHURCHILL & CHU 1975).

Now that this step has been accomplished, a more complete set of calculations is planned that reflects the thermal performance of the reference repository design. As initial conditions to these calculations, updated canister surface temperatures for HLW and SF at the time of emplacement are needed.

The objective of this memorandum is to update the estimation of the canister surface temperature, both for HLW and SF, taking into account the most recent data for heat output, thermal conductivity and canister geometries.

2 Conceptual model

The conceptual model assumptions can be summarised as follows:

- Steady-state conditions
- Homogeneous heat generation within the canister
- Radial heat conduction in canister wall
- Radiation of heat from canister surface to air
- Constant temperature in air, corresponding to ambient rock temperature at repository depth (perfect mixing tank)

Fig. A-1 shows a cross-section through the canister and the main heat transfer processes involved. Radiation from the canister surface to air is described by the Stefan-Boltzmann law (CARSLAW & JAEGER 2000):

$$S \sigma E (T_s^4 - T_{air}^4) = Q$$

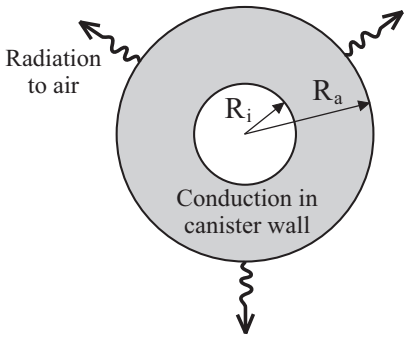

Fig. A-1: Model geometry and heat transfer processes

with

S	$= 2 \pi R_a (R_a + L)$ Canister surface [m^2]
L, R_a	Canister length and outer radius [m]
σ	Stefan-Boltzmann constant ($= 5.67 \cdot 10^{-8}$ $Wm^{-2}K^{-4}$)
E	Emissivity[1] [-]
T_s, T_{air}	Temperature of canister surface and air [K]
Q	Total heat production rate within canister [W]

Solving for T_s yields

$$T_s = (T_{air}^4 + Q / (S \sigma E))^{1/4} \quad (1)$$

Eq. (1) means that the heat production rate Q is the only parameter internal to the canister needed for the calculation of the surface temperature T_s.

The temperature profile within the canister wall for steady-state conditions is described by Laplace's equation:

$$\Delta T = 0 \quad (2)$$

Solving Eq. (2) in radial coordinates, i.e. neglecting the effect of the finite length of the canister, and imposing $T(R_a) = T_s$ yields

$$T(r) = T_s - Q / (2\pi\lambda L) \ln (r/R_a) \quad (3)$$

with

λ Thermal conductivity of the canister wall [W/(mK)]

[1] The emissivity is defined as the ratio of the heat emitted by a given body to that emitted by a black body (= perfect emittor) at the same temperature.

3 Input data

The input data set used for the calculation of the canister surface temperature is listed in Table A I-1.

Table A-1: Input data set used for the calculation of the surface temperature of HLW/SF canisters

Parameter	Symbol	Unit	Value	Comment
Canister length	L	m	2.0 5.0	HLW SF
Canister outer radius	R_a	m	0.47 0.525	HLW SF
Thermal conductivity of canister wall (steel)	λ	W/(mK)	52	HLW/SF
Emissivity	E	-	0.6-0.7 0.02-0.05 0.03-0.1	oxidised metal surfaces[1] polished metal surfaces[1] clean copper surface[2]
Heat output	Q	W	538 688 1500	HLW (COGEMA) HLW (BNFL) SF
Ambient temperature (air)	T_{air}	°C	38	Taken to be equal to the ambient rock temperature in the Opalinus clay at a depth of 650 m

[1] CARSLAW & JAEGER (2000), p. 21
[2] SKB (1999), p. 62

4 Results

Little uncertainty exists on heat output of SF/HLW, thermal conductivity of steel and canister geometries. Therefore, no parameter variations have been carried out for these parameters.

The emissivity of metal surfaces is a major source of uncertainty in the reported results on canister surface temperatures. As indicated in Table 1, the emissivity of metal surfaces varies between 0.02 and 0.7, depending on the given metal type and on the state of its surface. In the case of the oxidised surfaces (emissivity ~0.7) of the SF/HLW steel canisters, the obtained surface temperatures are in the order of 52 – 56°C, as indicated in Table 2. For polished non-oxidised surfaces (e.g. clean copper surfaces), the calculated temperatures are significantly higher.

Table A-2: Canister surface temperatures (in °C) as a function of emissivity

Emissivity [-]	0.7	0.6	0.1	0.05	0.03	0.02
HLW (COGEMA)	52.4	54.6	113.6	160.6	206.1	249.2
HLW (BNFL)	56.1	58.8	128.4	181.3	231.4	278.4
SF	53.9	56.4	120.0	169.5	217.1	261.9

5 References

CARSLAW, H. S. & JAEGER, J. C. (2000): Conduction of heat in solids. Oxford university press , Oxford, England. Second edition (2000).

CHURCHILL, S. W. & CHU, H. S. (1975): Correlating equations for laminar and turbulent free convection from a horizontal cylinder. Int. J. Heat Mass Transfer **18**, 1049.

SKB (1999): SR 97 – Processes in the repository evolution. SKB Techn. Report TR-99-07. SKB, Stockholm, Sweden.

HOPKIRK, R. J. & WAGNER, W. H. (1985): Thermal loading in the near-field of repositories for high-level and intermediate-level nuclear waste. Nagra Techn. Report NTB 85-54. Nagra, Wettingen, Switzerland.

SATO, R., SASAKI, T., ANDO, K., SMITH, P:A: & SCHNEIDER, J:W: (1998): Calculations of the temperature evolution of a repository for spent fuel in crystalline and sedimentary rocks. Nagra Techn. Report NTB 97-02. Nagra, Wettingen, Switzerland.

Appendix B

Appendix B: Comparison of diffusive and convective heat transport rates in dry Bentonite

The objective of this note is to estimate the contributions of pure conduction and free (natural) convection to heat transport within dry bentonite emplaced around SF canisters. Fig. 1 illustrates the geometry and the transport processes under investigation.

1 Heat conduction

The quantitative estimate of the heat conduction rate is based on the following conceptual assumptions:

- Step-wise steady-state conditions
- Radially symmetric heat conduction assuming fixed temperatures at the inner/outer boundary of bentonite.

The conductive heat transport rate, F_{cond} [W], can be calculated from:

$$F_{cond} = 2\pi L\lambda \frac{\Delta T}{\ln \frac{R_T}{R_C}} \qquad \text{(Eq. 1)}$$

with

L	canister length [m]
λ	thermal conductivity of dry bentonite [W/mK]
ΔT	temperature difference between inner/outer boundary of bentonite [K]

2 Heat convection

The quantitative estimate of the heat convection rate is based on the following conceptual assumptions:

- Step-wise steady-state conditions
- Dry bentonite (ca. 2% moisture content)
- Free (natural) convection of air is driven by temperature difference between canister and bentonite (assumed to be roughly equal to the temperature difference in bentonite above/below the canister)
- Heat is taken up by air moving upwards near the canister wall and released by air moving downwards near the outer bentonite boundary (Fig. A II-1). Thereafter, heat is transported away by pure conduction in saturated Opalinus Clay.

The net convective heat transport rate, F_{conv} [W], transported away by gas from the canister to the Opalinus Clay, can be calculated from:

$$F_{conv} = \dot{n}\ C_V \Delta T \qquad \text{(Eq. 2)}$$

with

$\dot{n}$	number of moles of air passing by the canister per unit time [mol/s]
C_V	molar heat capacity of air [J/mol K]
ΔT	temperature difference between upper/lower part of bentonite [K]

The flow of air is calculated by combining Darcy's law with the universal gas law (at fixed total air volume):

$$\dot{n} = 2\frac{k_g}{\eta_g}\frac{\Delta p}{\Delta l}\frac{S}{V_{mol}} = 2\frac{k_g}{\eta_g}\frac{\bar{p}}{\pi R_C}\frac{\Delta T}{\bar{T}}\frac{L\dfrac{R_T - R_C}{2}}{\dfrac{R\bar{T}}{\bar{p}}} = \frac{k_g L(R_T - R_C)}{\pi\ \eta_g R_C R}\left(\frac{\bar{p}}{\bar{T}}\right)^2 \Delta T \quad \text{(Eq. 3)}$$

with

k_g	permeability of air in dry bentonite [m^2]
η_g	viscosity of air at mean temperature [Pa s]
Δp	gas pressure difference induced by temperature difference [Pa]
Δl	length over which Δp is maintained [m]
$\bar{p}, \bar{T}$	mean gas pressure and mean temperature in bentonite [Pa]
S	cross-sectional area perpendicular to upwards directed gas flow [m^2]
V_{mol}	molar volume of air at mean temperature [m^3/mol]
R	universal gas constant [J/mol K]

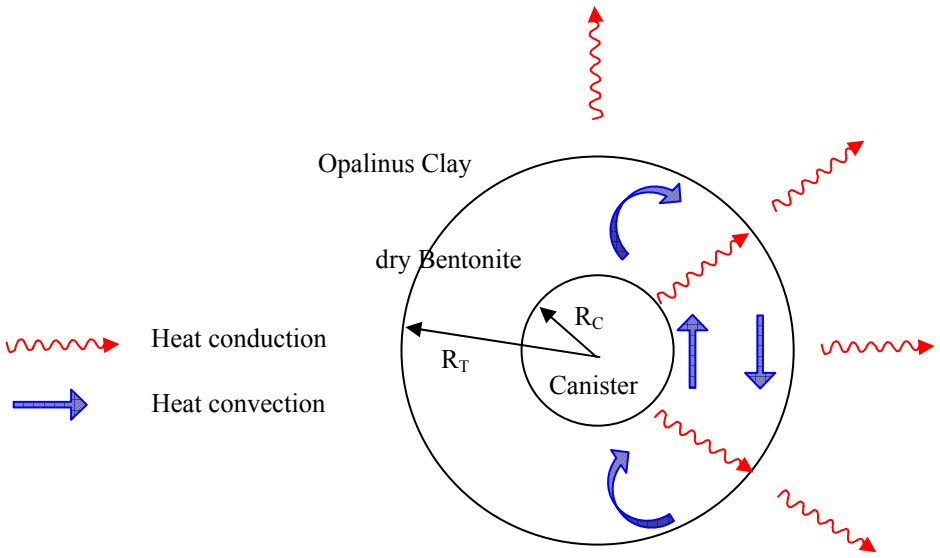

Fig. B-1: Sketch of heat transport processes within dry bentonite around SF canisters

3 Input data

Table B-1: Referenced input data used in model heat transport calculations

Parameter	**Symbol**	**Unit**	**Value**	**Reference**
Canister length	L	m	4.7	
Canister radius	R_C	m	0.525	
Tunnel radius	R_T	m	1.25	
Thermal conductivity of dry bentonite	λ	W/m K	0.4	
Permeability of air in dry bentonite (mixture of powder and pellets at 3.5% moisture content)	k_g	m^2	1E-12	VOLCKAERT (1996)
Molar heat capacity of air	C_V	J/mol K	2.5 R	KNEUBÜHL (1982)
Viscosity of air at mean temperature	η_g	Pa s	2.2E-05	
Mean gas pressure in bentonite	$\overline{p}$	Pa	1.4E+05	rough estimate, (based on p/T=const.)
Mean temperature in bentonite	$\overline{T}$	K	373	
Heat output of SF canister (reference UO_2/MOX canister)	P	W	1500 (t=0a) 696 (t=100a) 177 (t=1000a)	MCGINNES (2002)

4 Results

The estimated contributions of pure thermal conduction and free convective heat transport in dry bentonite are compared in Fig. B-2. In the case of free convection, the reference value for the gas permeability is 10^{-12} m^2 (VOLCKAERT 2000), but is varied from $k_g = 10^{-11}$ to 10^{-13} m^2. Also shown is the heat output rate of a single UO_2/MOX spent fuel canister at the time of emplacement (t=0), as well as at 100 a and 1000 a after emplacement.

The canister heat output can be transported away by pure conduction, if the following temperature differences are maintained (step-wise in time) between the canister surface and the bentonite/Opalinus Clay interface:

- ca. 100 K at time t = 0 a
- ca. 50 K at time t = 100 a
- ca. 10 K at time t = 1000 a

These temperature differences between canister surface and interface bentonite/Opalinus Clay qualitatively agree with transient numerical model calculations on temperature evolution in the spent fuel repository, assuming heat conduction only.

Based on the reference value for the gas permeability of dry bentonite, the estimated contribution of free convection to total heat transport is in the order of 25% at most (Fig. 2). In the case of an increased gas permeability of dry bentonite in the order of 10^{-11} m^2, free convection contributes significantly to cooling of bentonite.

5 Summary and conclusions

The radiogenic heat produced inside the spent fuel canister is transported through bentonite predominantly by heat conduction. A temperature difference between inner/outer parts of bentonite of roughly 100°C is established at early times after closure, leading to absolute temperatures well above 100°C in the inner half of the bentonite layer.

The contribution of heat transport by circulating air inside dry bentonite (free convection) amounts at most to 25% of the total heat transport. This is due to the relatively modest gas permeability of dry bentonite (ca. 10^{-12} m^2). It is only for increased gas permeabilities in the order of 10^{-11} m^2, or higher, that free convection could noticeably reduce the elevated temperatures in the inner part of bentonite.

6 References

KNEUBÜHL, F. (1982): Repetitorium der Physik. Teubner Studienbücher, Stuttgart (1982).

McGINNES, D. F. (2002): Model radioactive waste inventory for reprocessing waste spent fuels, Nagra Technical Report NTB 01-01.

VOLCKAERT G., BERNIER, F., ALONSO, E. et al. (1996): Thermal-hydraulic-mechanical and geochemical behaviour of the clay barrier in radioactive waste repositories (model development and validation): final report. EUR 16744 EN., European Commission, Brussels.

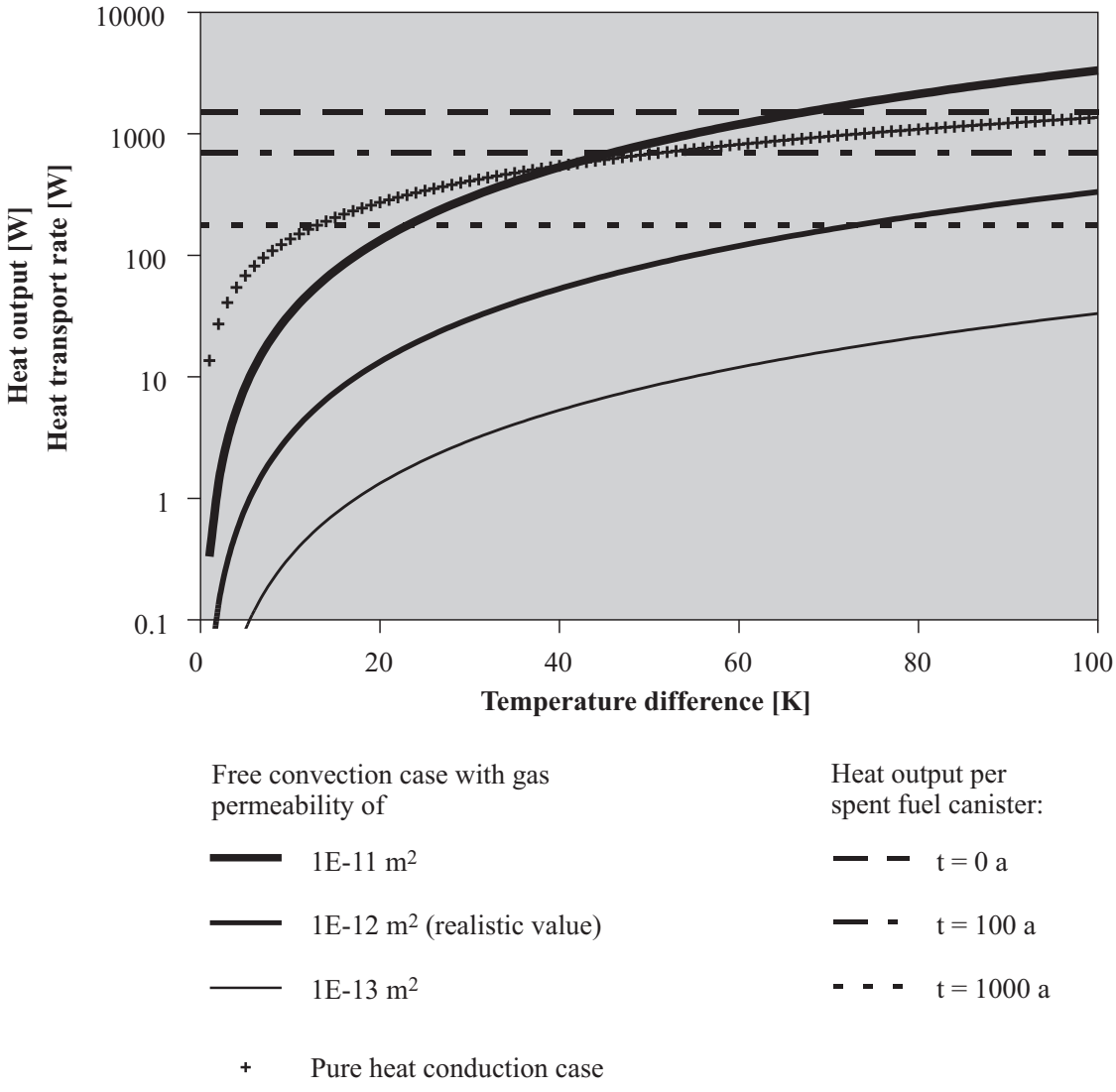

Fig. B-2: Comparison of spent fuel canister heat output and heat transport by pure conduction and free convection within dry bentonite

Appendix C

Temperature-time evolution in the vertical and horizontal orientations and temperature distributions at various times for SF and HLW emplacement tunnels

(Figures)

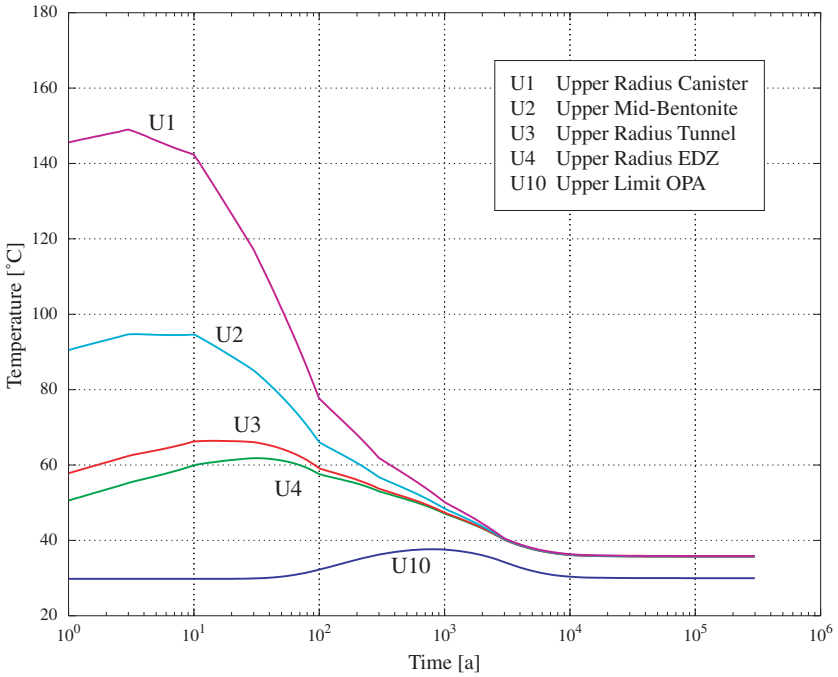

Fig. C-1: The time-dependent temperature distribution in the vertical plane above the emplacement tunnels for HLW canisters for the case of low bentonite thermal conductivity (low moisture content). (see Figs 9 and 10 for the locations at which temperatures are plotted).

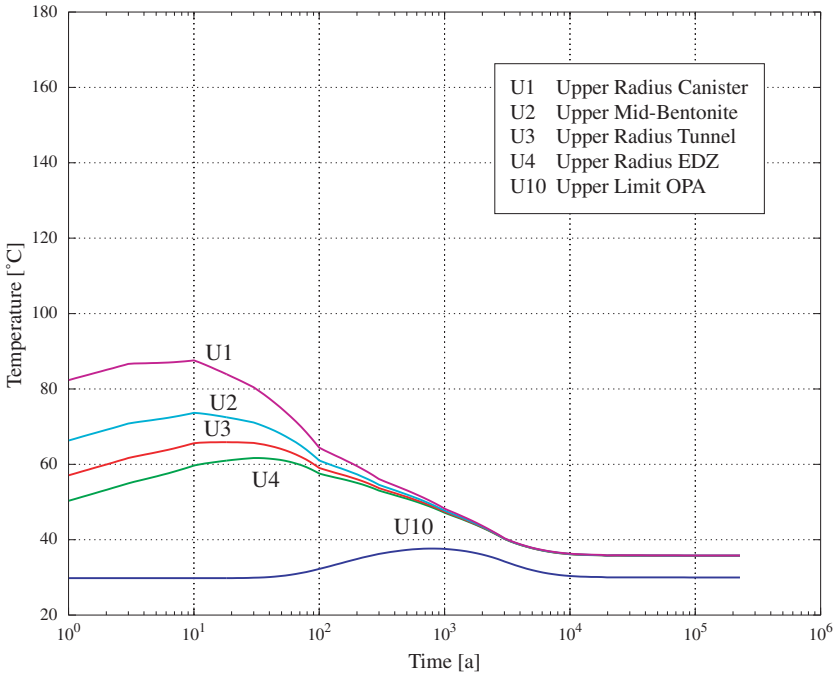

Fig. C-2: The time-dependent temperature distribution in the vertical plane above the emplacement tunnels for HLW canisters for the case of high bentonite thermal conductivity (high moisture content). (see Figs 9 and 10 for the locations at which temperatures are plotted).

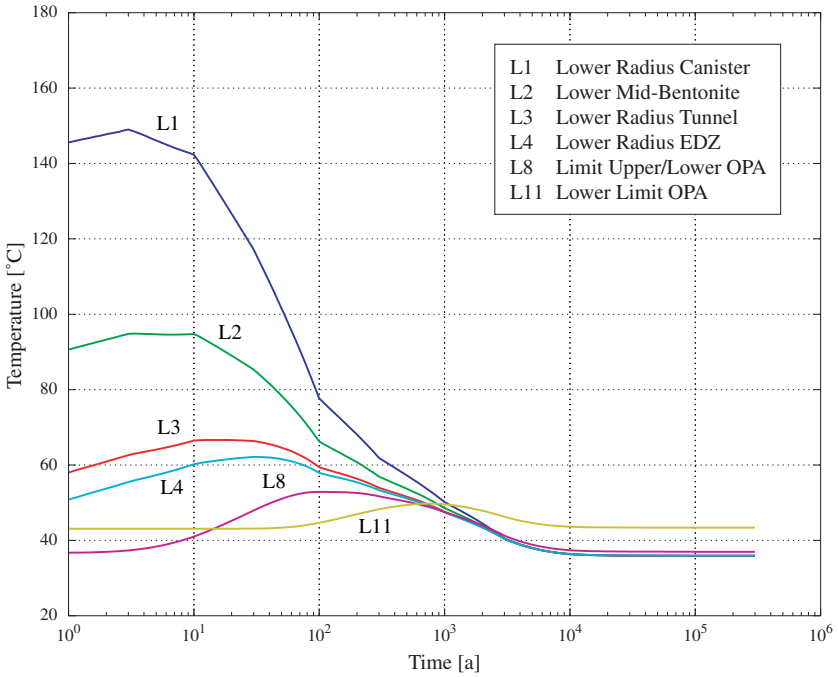

Fig. C-3: The time-dependent temperature distribution in the vertical plane below the emplacement tunnels for HLW canisters for the case of low bentonite thermal conductivity (low moisture content). (see Figs 9 and 10 for the locations at which temperatures are plotted).

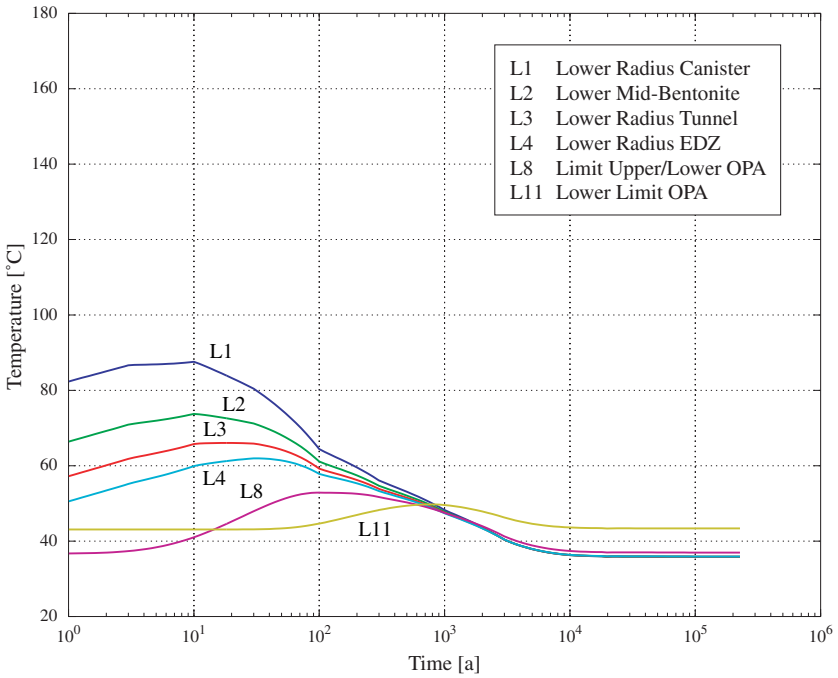

Fig. C-4: The time-dependent temperature distribution in the vertical plane below the emplacement tunnels for HLW canisters for the case of high bentonite thermal conductivity (high moisture content). (see Figs 9 and 10 for the locations at which temperatures are plotted).

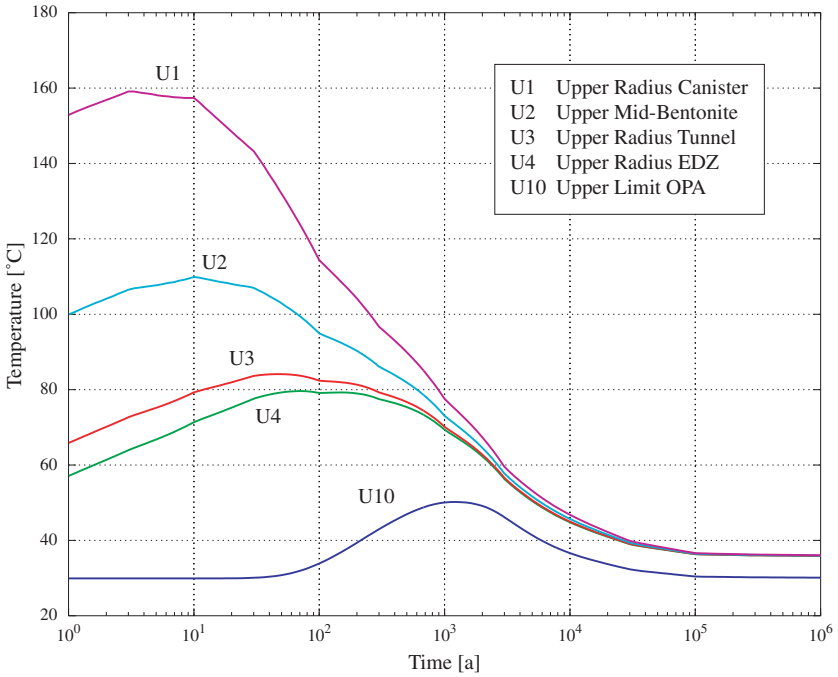

Fig. C-5: The time-dependent temperature distribution in the vertical plane above the emplacement tunnels for UO_2 fuel canisters for the case of low bentonite thermal conductivity (low moisture content). (see Figs 9 and 10 for the locations at which temperatures are plotted).

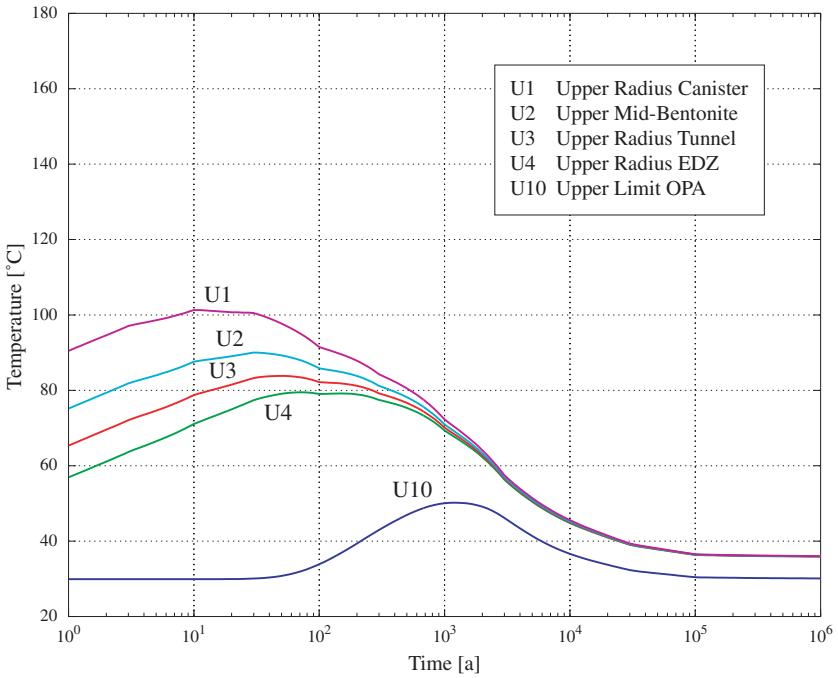

Fig. C-6: The time-dependent temperature distribution in the vertical plane above the emplacement tunnels for UO_2 fuel canisters for the case of high bentonite thermal conductivity (high moisture content). (see Figs 9 and 10 for the locations at which temperatures are plotted).

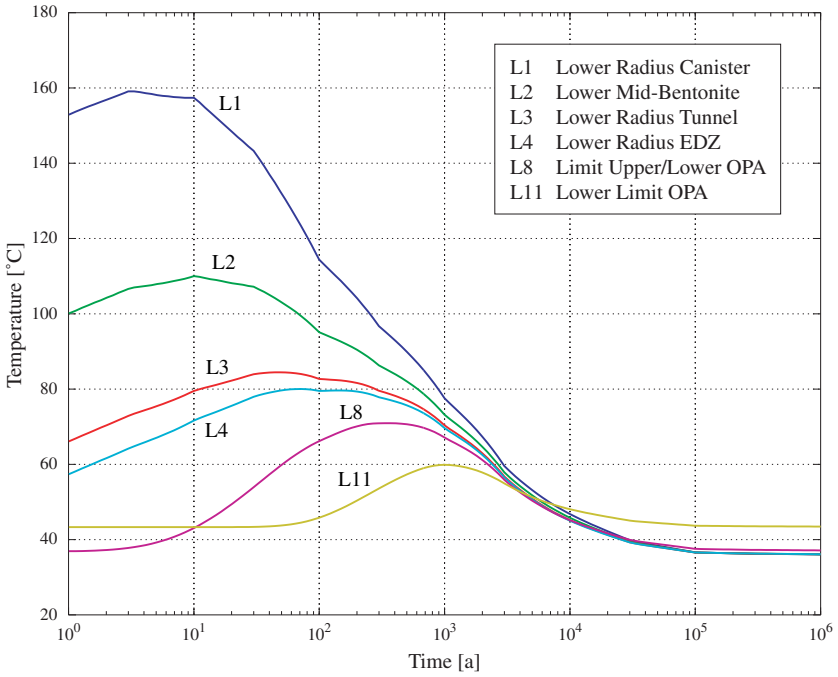

Fig. C-7: The time-dependent temperature distribution in the vertical plane below the emplacement tunnels for UO_2 fuel canisters for the case of low bentonite thermal conductivity (low moisture content). (see Figs 9 and 10 for the locations at which temperatures are plotted).

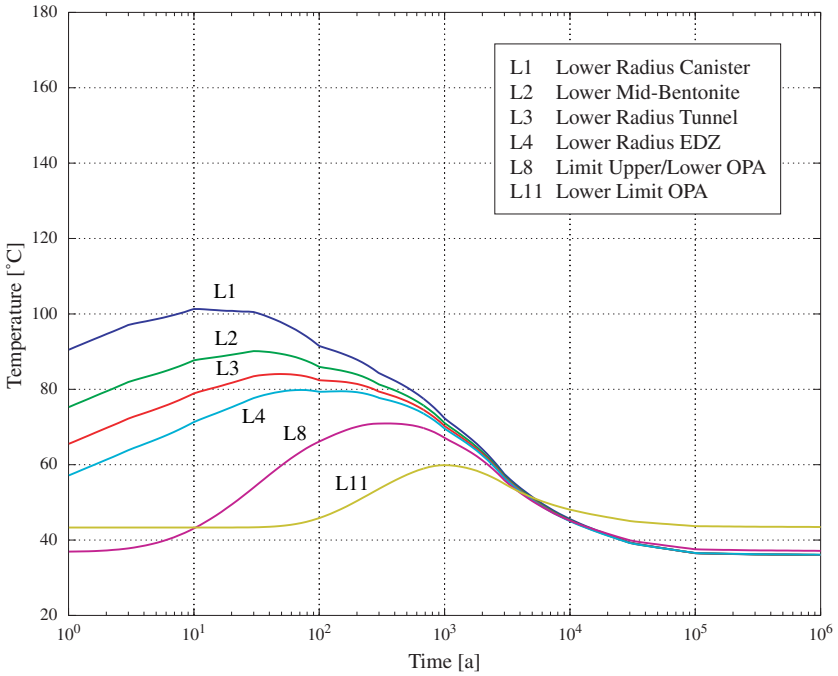

Fig. C-8: The time-dependent temperature distribution in the vertical plane below the emplacement tunnels for UO_2 fuel canisters for the case of high bentonite thermal conductivity (high moisture content). (see Figs 9 and 10 for the locations at which temperatures are plotted).

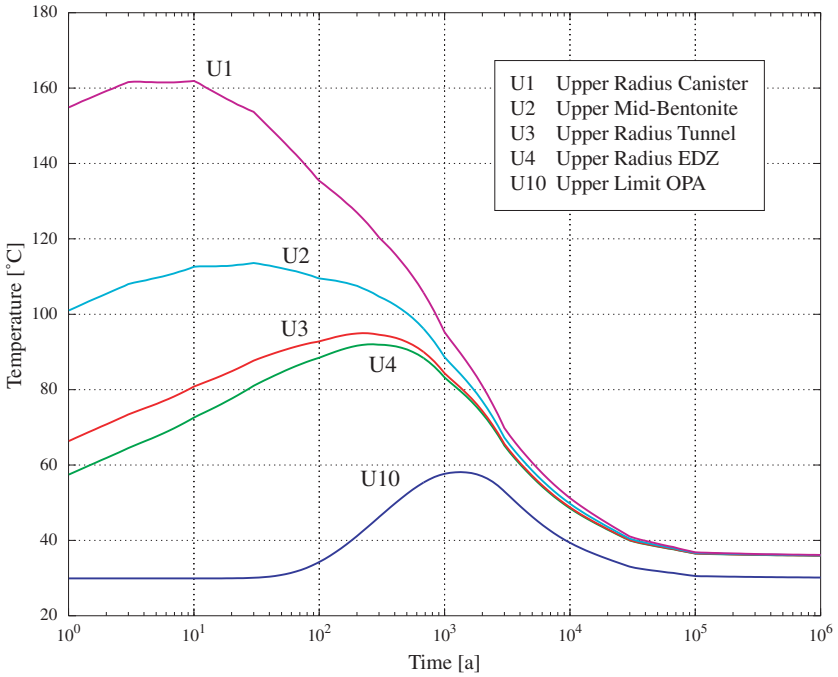

Fig. C-9: The time-dependent temperature distribution in the vertical plane above the emplacement tunnels for MOX/UO_2 fuel canisters for the case of low bentonite thermal conductivity (low moisture content). (see Figs 9 and 10 for the locations at which temperatures are plotted).

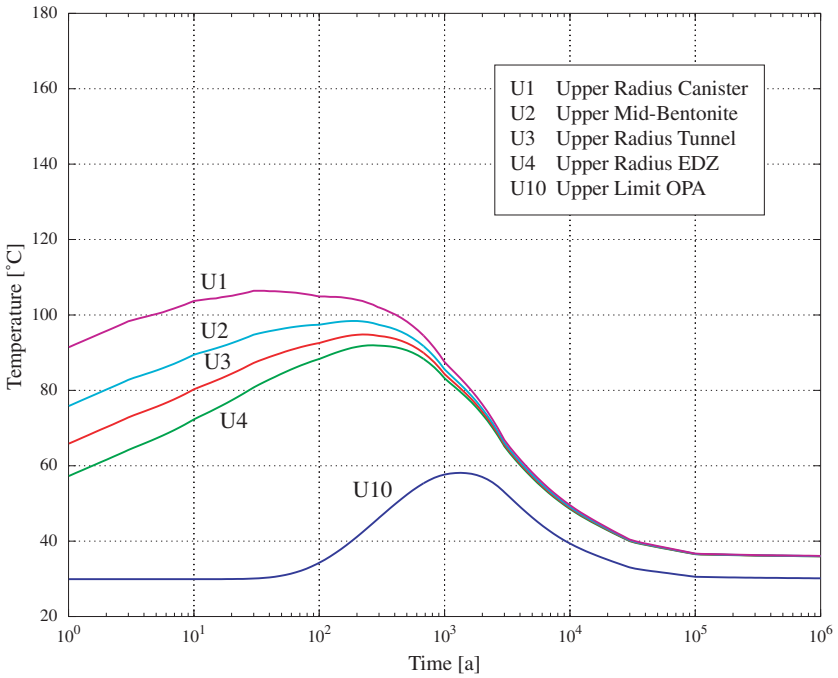

Fig. C-10: The time-dependent temperature distribution in the vertical plane above the emplacement tunnels for MOX/UO_2 fuel canisters for the case of high bentonite thermal conductivity (high moisture content). (see Figs 9 and 10 for the locations at which temperatures are plotted).

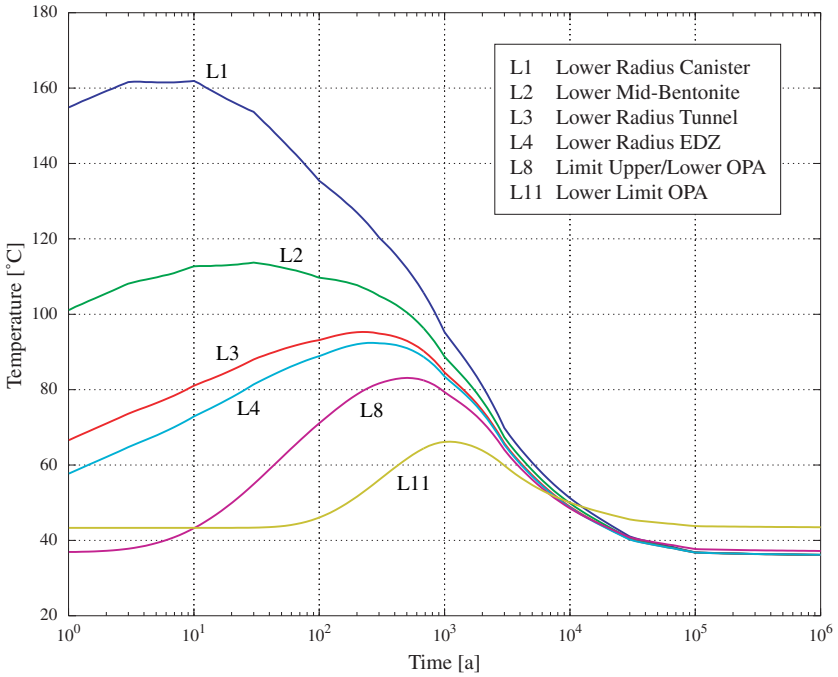

Fig. C-11: The time-dependent temperature distribution in the vertical plane below the emplacement tunnels for MOX/UO_2 fuel canisters for the case of low bentonite thermal conductivity (low moisture content). (see Figs 9 and 10 for the locations at which temperatures are plotted).

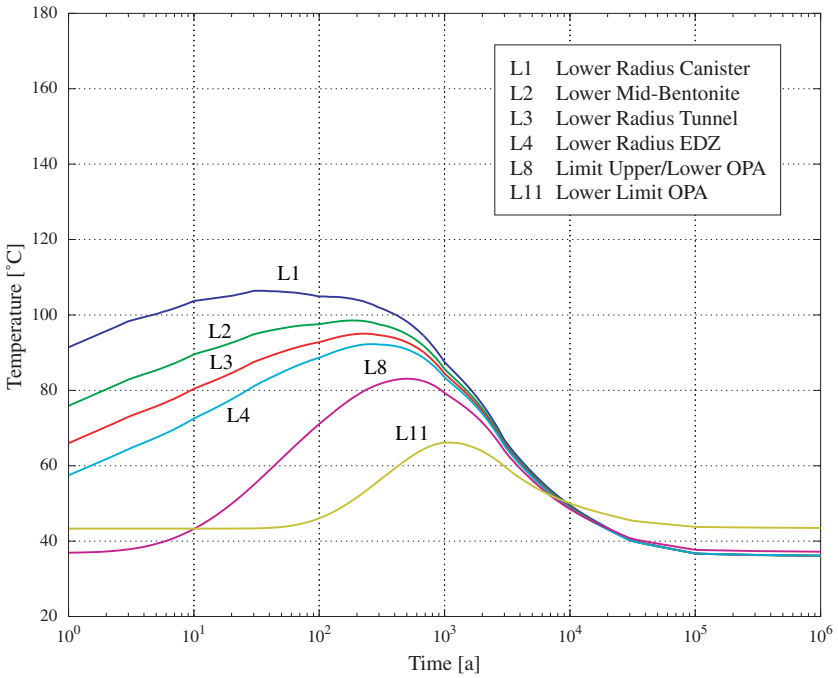

Fig. C-12: The time-dependent temperature distribution in the vertical plane below the emplacement tunnels for MOX/UO_2 fuel canisters for the case of high bentonite thermal conductivity (high moisture content). (see Figs 9 and 10 for the locations at which temperatures are plotted).

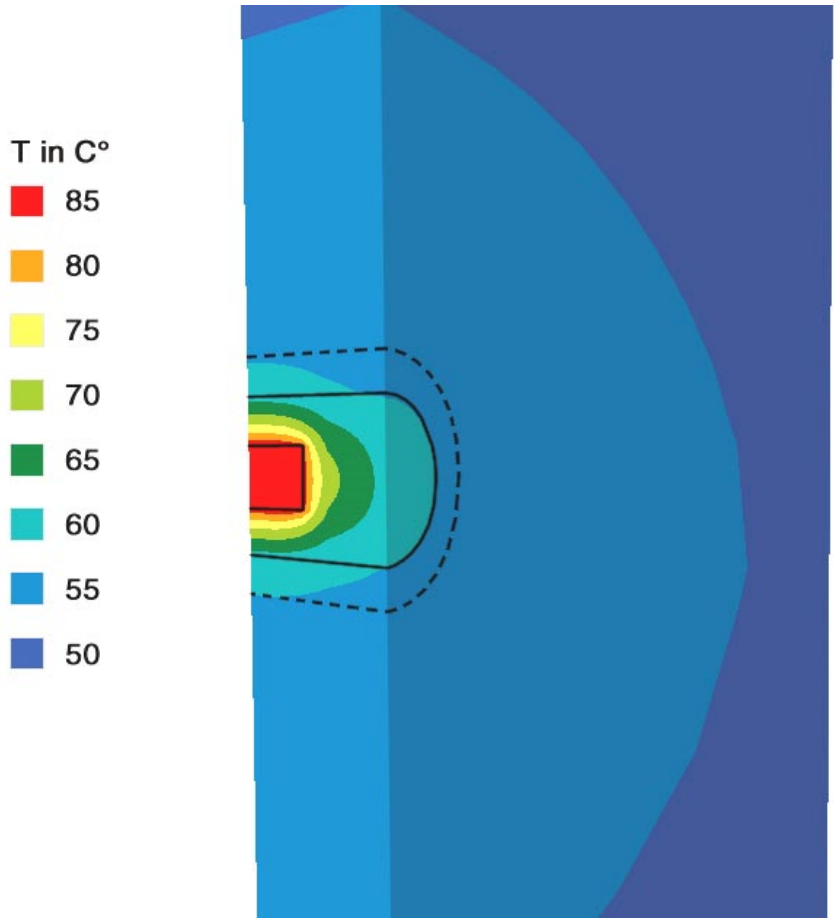

Fig. C-13: Temperature profiles 57 years after emplacement, for a disposal tunnel with HLW canisters, for a low bentonite thermal conductivity (low moisture content). The canister is represented by the rectangle at the centre of the tunnel and the solid and dashed lines represent the tunnel boundary (R = 1.25 m) and the assumed outer boundary of the EDZ (R = 1.75 m), respectively. The vertical cross-sections are at mid-tunnel and midway between canisters.

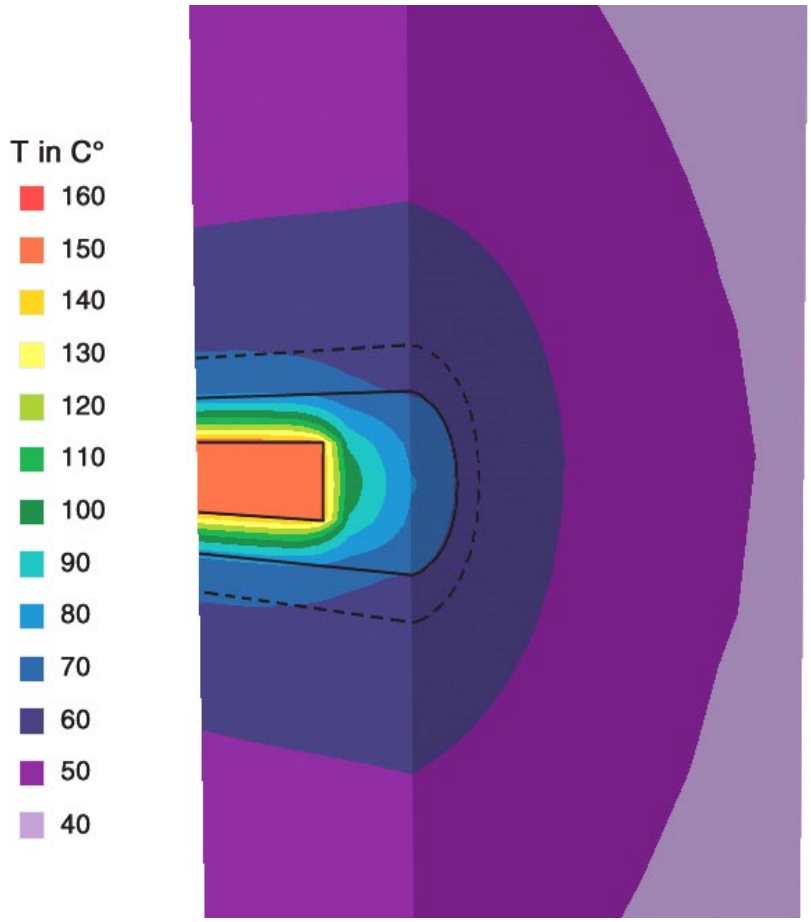

Fig. C-14: Temperature profiles 10 years after emplacement, for a disposal tunnel with UO_2 canisters, for a low bentonite thermal conductivity (low moisture content). The canister is represented by the rectangle at the centre of the tunnel and the solid and dashed lines represent the tunnel boundary (R = 1.25 m) and the assumed outer boundary of the EDZ (R = 1.75 m), respectively. The vertical cross-sections are at mid-tunnel and midway between canisters.

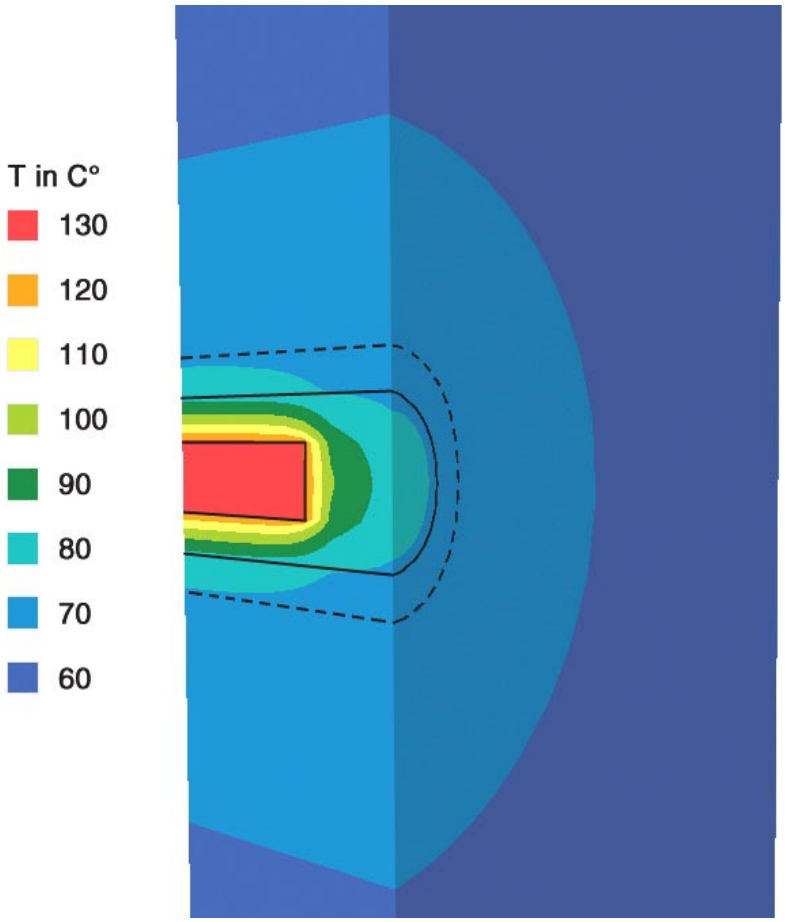

Fig. C-15: Temperature profiles 48 years after emplacement, for a disposal tunnel with UO_2 canisters, for a low bentonite thermal conductivity (low moisture content). The canister is represented by the rectangle at the centre of the tunnel and the solid and dashed lines represent the tunnel boundary (R = 1.25 m) and the assumed outer boundary of the EDZ (R = 1.75 m), respectively. The vertical cross-sections are at mid-tunnel and midway between canisters.

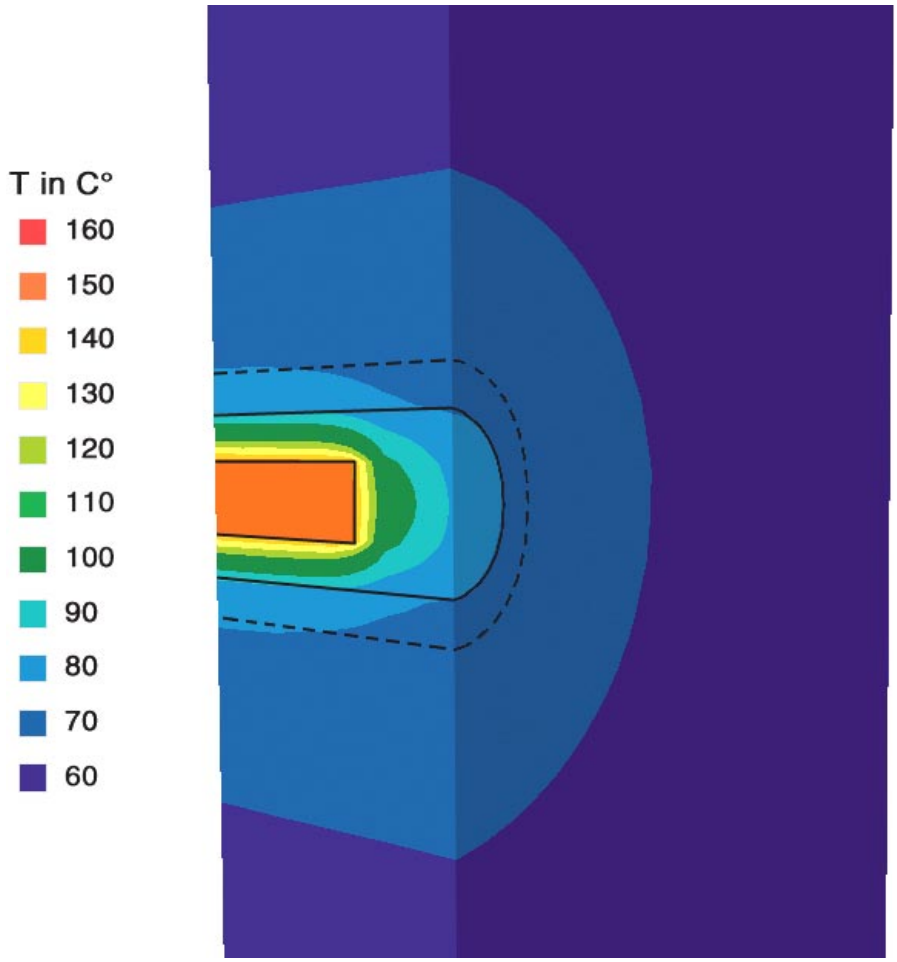

Fig. C-16: Temperature profiles 30 years after emplacement, for a disposal tunnel with MOX/UO_2 canisters, for a low bentonite thermal conductivity (low moisture content). The canister is represented by the rectangle at the centre of the tunnel and the solid and dashed lines represent the tunnel boundary (R = 1.25 m) and the assumed outer boundary of the EDZ (R = 1.75 m), respectively. The vertical cross-sections are at mid-tunnel and midway between canisters.

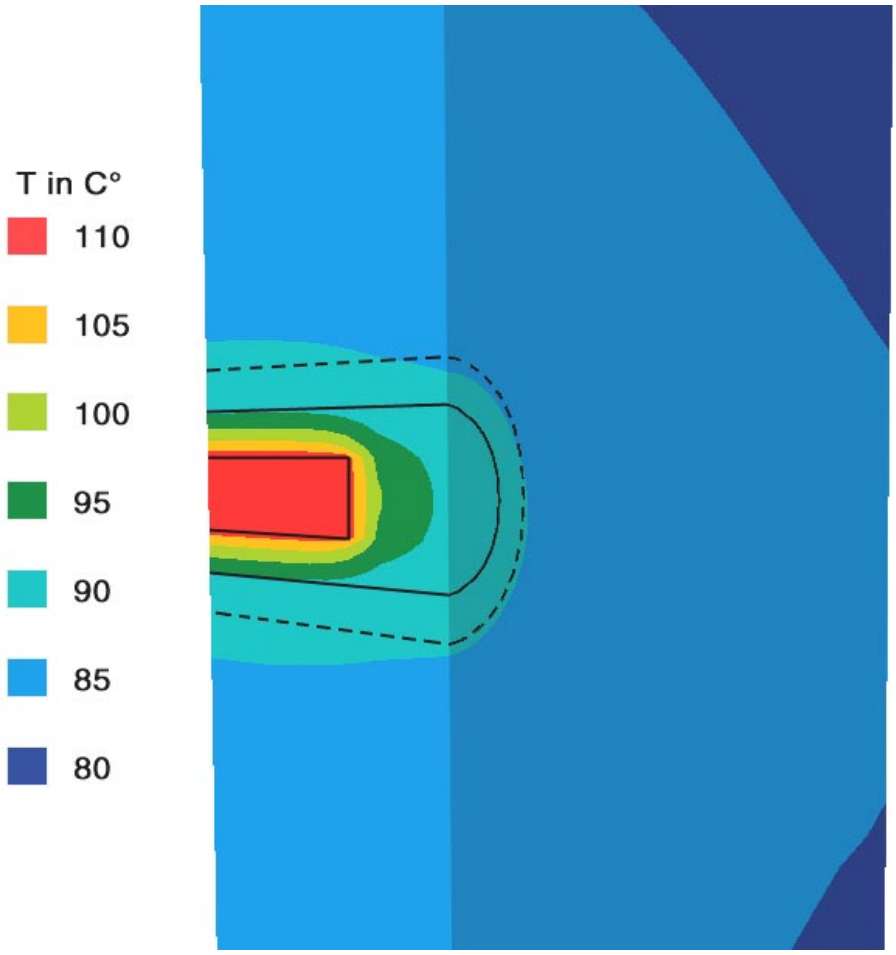

Fig. C-17: Temperature profiles 450 years after emplacement, for a disposal tunnel with MOX/UO_2 canisters, for a low bentonite thermal conductivity (low moisture content). The canister is represented by the rectangle at the centre of the tunnel and the solid and dashed lines represent the tunnel boundary (R = 1.25 m) and the assumed outer boundary of the EDZ (R = 1.75 m), respectively. The vertical cross-sections are at mid-tunnel and midway between canisters.

Appendix D

Temperature evolution for intermediate-level waste emplacement tunnels

Temperature evolution for intermediate-level waste emplacement tunnels

1 Introduction

Heat in the ILW tunnels is produced by radioactive decay of the waste and cement hydration processes following tunnel backfilling. Analytical steady-state calculations of the temperature distribution within and around the ILW tunnels have been performed using a radially symmetric model for the tunnel cross-section. An additional calculation was performed for the reference case using a numerical steady-state model based on slightly different conceptual assumptions (2 tunnels with 100 m spacing embedded in a larger model area). The numerical calculations were carried out using the Method of Boundary Elements (Code BEASY).

2 Calculation of the temperature rise due to radioactive decay

The model cross-section consists of three domains, each with a depth of 1 m:

Domain 1: Emplacement container and waste
Domain 2: Tunnel liner and backfill
Domain 3: Opalinus Clay (including EDZ)

In one of the parameter variations, an additional domain serves to investigate the role of air gaps between domains 1,2 and 2,3 respectively (see below). The radiogenic heat generation within domain 1 is 26.7 W per unit length of tunnel. The ambient temperature of the host rock at a repository depth of 650 m is 38°C.

Parameter variations

- increased heat generation (118.5 W/m instead of 26.7 W/m)
- 40% reduction of thermal conductivity of Opalinus Clay
- air gaps of 0.01 m aperture between domains 1,2 and 2,3.

3 Calculation of the temperature rise due to cement hydration

During the first day after backfilling approximately 50% of the total hydration heat of 2.55 GJ are released. The corresponding temperature rise can be estimated by assuming rapid transport and homogenisation of heat in domains 1 and 2 (mixing tank).

4 Results and conclusions

The maximum temperature in the ILW repository caused by radioactive decay is 44°C (Reference Case, see Fig. D-1). The numerical calculations for the Reference Case yield a slightly higher temperature of 49°C, due to differences in the conceptual model. For the investigated parameter variations, the maximum temperatures are 64°C (increased heat generation), 47°C (reduced thermal conductivity of OPA) and 45°C (air gaps). In parallel with radioactive decay these excess temperatures decrease with time.

The hydration heat released during hardening of the cementitious backfill mortar leads to a maximal temperature in the ILW repository of 50°C. This temperature peak is of short duration (a few weeks to months).

In view of these results, the conclusion may be drawn that the effects of heat generation by radioactive decay and cement hydration on the ILW repository are marginal.

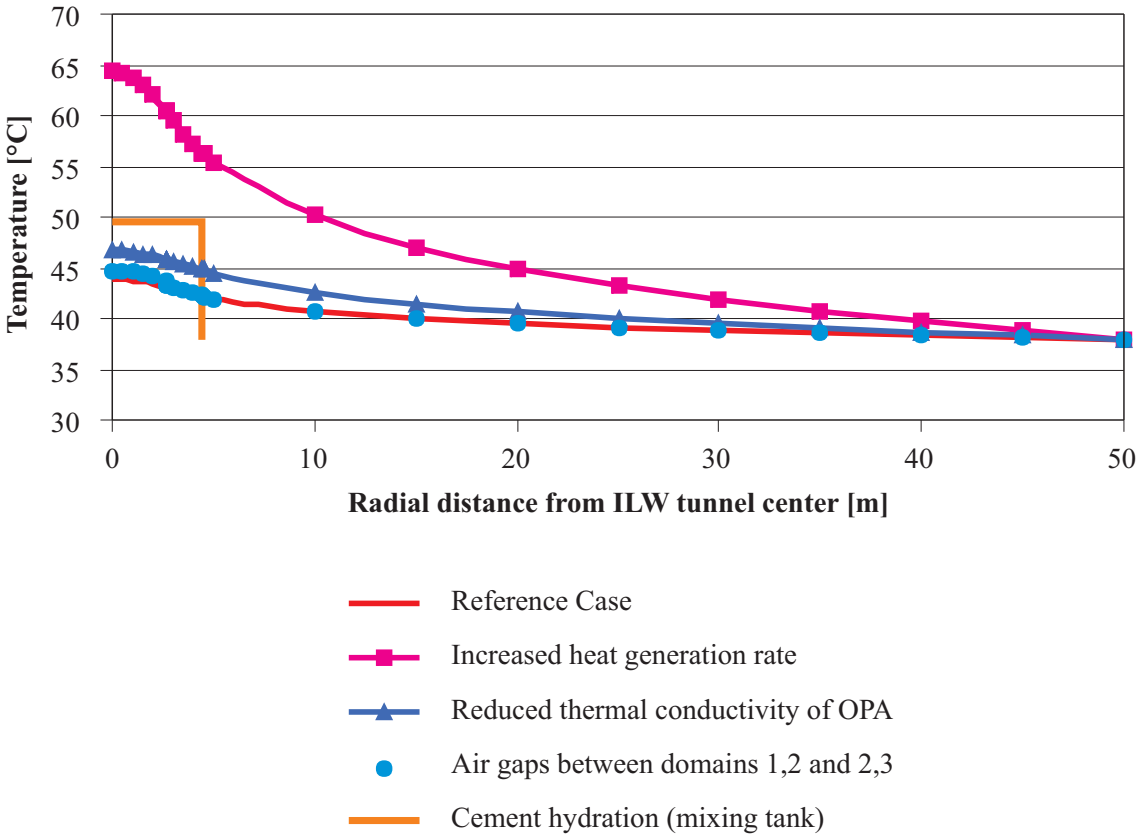

Fig. D-1: Analytically calculated radial temperature profiles within and in the vicinity of an ILW emplacement tunnel located in the Opalinus Clay

Appendix E

SF/OPA thermal evolution: Analytical benchmark

The objective of this note is to provide a benchmark for the thermal calculations for SF in the Opalinus Clay. The following case was chosen:

- saturated bentonite MOX/UO_2
- reference point U10 ("upper limit OPA, z = -550 m")

The case was selected, because the U10 position is sufficiently far above the emplacement tunnels (see Fig. III-10) that the array of tunnels approximate a planar heat source, thus simplifying the analytical solution.

The conceptual assumptions, input data and results are summarised in Tables E-1 and E-2 and Fig. E-1. The results of the comparison between the analytical results and the finite-element calculation for the U10 position are shown in Fig. 17.

In conclusion, a good agreement was found between the numerically and analytically calculated temperature 100 m above the SF repository.

Table E-1: SF thermal evolution: Parameters for Analytical benchmark

Heat source term	W	612.39	W/canister	derived from exponential regression curve
Decay constant	lam	1.45E-03	1/a	derived from exponential regression curve
Canister radius	a	0.525	m	
Canister pitch	p	7.7	m	
Tunnel separation	d	40	m	
Heat capacity OPA	c	2.30E+06	J/m3K	
Thermal conductivity OPA	lambda	1.8	W/mK	
Position	zz	100	m	
Environ. Temperature	T00	38	C	
Geothermal gradient	g	0.08	C/m	
Seconds per year	spy	3.16E+07	s/a	
Calculations:				
Thermal diffusivity	kappa	7.8E-07	m2/s	(= Conductivity/Capacity)
Averaged heat flux	Q	9.9E-01	W/m2	(only half of heat flux is directed upwards)

Vertical temperature profile calculated analytically using CARSLAW & JAEGER, p.76 (Eq. 9):

- o Bentonite and OPA are modelled as a 1D semi-infinite, homogeneous medium (z>0)
- o Flux of heat from repository at z=0 is an exponentially decreasing function (best fit to heat output in time domain between 300 to 1'000 a)
- o Benchmark performed for point U10 (-550 m, upper limit OPA),

Table E-2: Heat output from reference UO2+MOX canister

Time from rep. closure [a]	Heat output [W]	Ln(Heat output) [ln(W)]	Lin. Regr.: Best exp-fit for time [W]	domain 300-1000a
0	1500	7.31	612	
3	1450	7.28	610	
10	1330	7.19	604	
30	1080	6.98	586	
100	696	6.55	530	
300	422	6.05	397	
1000	177	5.18	144	
3000	68	4.22	8	
1.00E+04	39	3.66	0	
3.00E+04	14	2.64	0	
1.00E+05	3	1.10	0	
			6.41737199	W= 612.39
			-0.00144817	lam= 1.45E-03

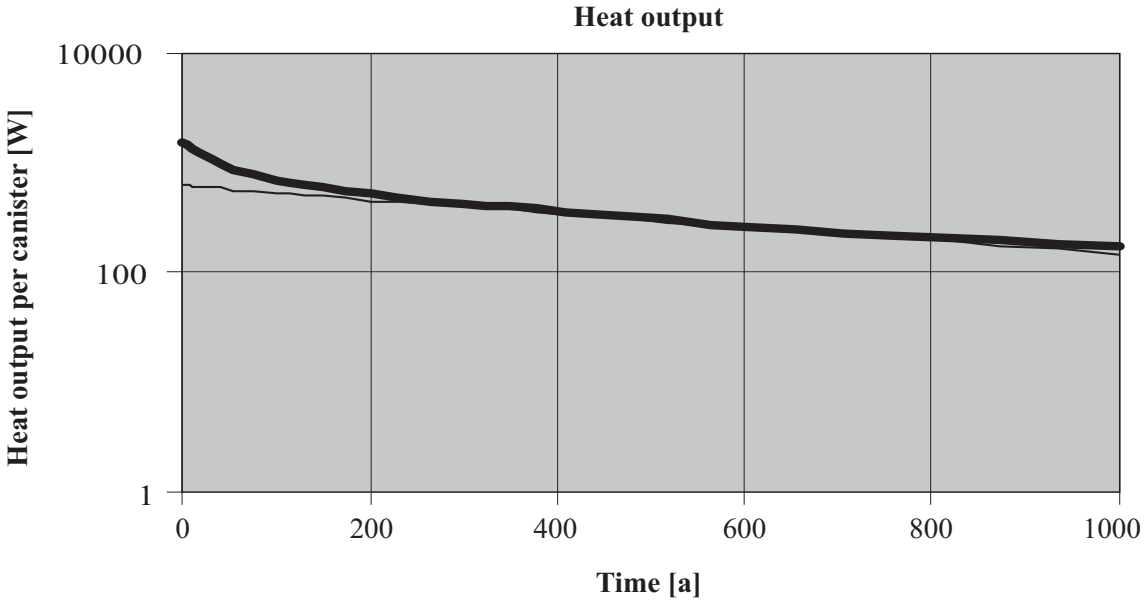

Fig. E-1: Heat Output of canister vs. time - actual (heavy line) and exponential fit

Calculations:

Canister	Unit	HLW		SF
		COGEMA	BNFL	
Surface temperature	°C	52.4	56.1	53.9

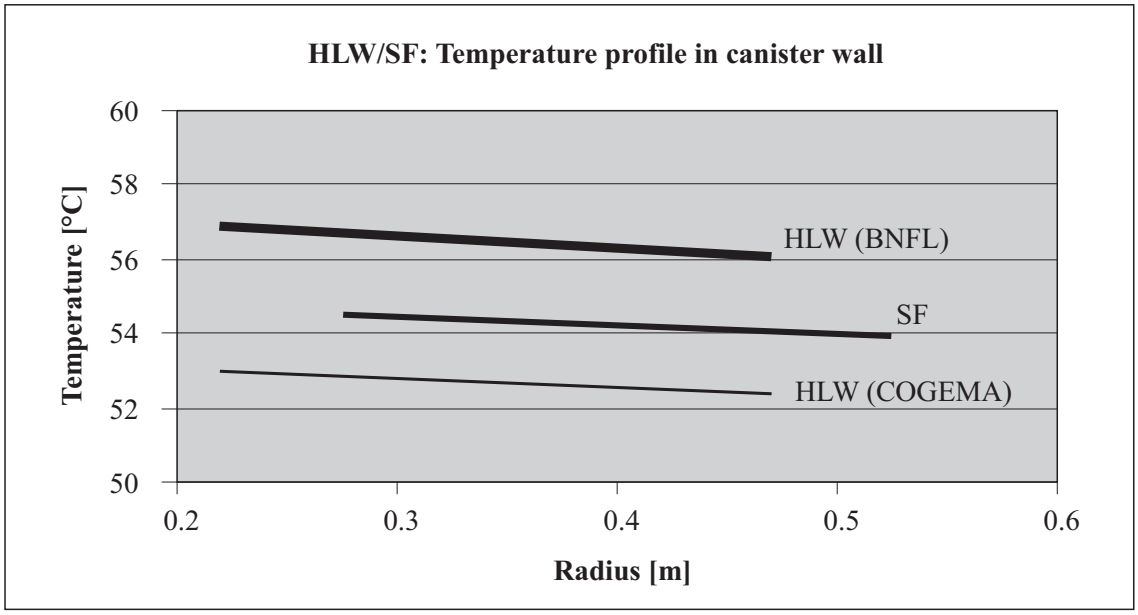

Fig. E-2: HLW/SF: Temperature profile in canister wall

Table E-3: Temperature profile in canister wall:

C	0.82		1.05		0.92	
DELTAR	0.25					
NUM	100					
Index	HLW (COGEMA)		HLW (BNFL)		SF	
	Radius	Temperature	Radius	Temperature	Radius	Temperature
	[m]	[°C]	[m]	[°C]	[m]	[°C]
0	0.22	53.02	0.22	56.88	0.275	54.54
1	0.2225	53.01	0.2225	56.87	0.2775	54.53
2	0.225	53.00	0.225	56.86	0.28	54.52
3	0.2275	52.99	0.2275	56.85	0.2825	54.51
4	0.23	52.98	0.23	56.84	0.285	54.50
5	0.2325	52.97	0.2325	56.83	0.2875	54.50
6	0.235	52.96	0.235	56.81	0.29	54.49
7	0.2375	52.96	0.2375	56.80	0.2925	54.48
8	0.24	52.95	0.24	56.79	0.295	54.47
9	0.2425	52.94	0.2425	56.78	0.2975	54.46
10	0.245	52.93	0.245	56.77	0.3	54.46
11	0.2475	52.92	0.2475	56.76	0.3025	54.45
12	0.25	52.91	0.25	56.75	0.305	54.44
13	0.2525	52.91	0.2525	56.74	0.3075	54.43
14	0.255	52.90	0.255	56.73	0.31	54.43
15	0.2575	52.89	0.2575	56.72	0.3125	54.42
16	0.26	52.88	0.26	56.71	0.315	54.41
17	0.2625	52.87	0.2625	56.70	0.3175	54.40
18	0.265	52.87	0.265	56.69	0.32	54.40
19	0.2675	52.86	0.2675	56.68	0.3225	54.39
20	0.27	52.85	0.27	56.67	0.325	54.38
21	0.2725	52.84	0.2725	56.66	0.3275	54.38
22	0.275	52.84	0.275	56.65	0.33	54.37
23	0.2775	52.83	0.2775	56.64	0.3325	54.36
24	0.28	52.82	0.28	56.63	0.335	54.36
25	0.2825	52.81	0.2825	56.62	0.3375	54.35
26	0.285	52.81	0.285	56.61	0.34	54.34
27	0.2875	52.80	0.2875	56.60	0.3425	54.34
28	0.29	52.79	0.29	56.59	0.345	54.33
29	0.2925	52.78	0.2925	56.58	0.3475	54.32
30	0.295	52.78	0.295	56.58	0.35	54.32
31	0.2975	52.77	0.2975	56.57	0.3525	54.31
32	0.3	52.76	0.3	56.56	0.355	54.30

C	0.82		1.05		0.92	
DELTAR	0.25					
NUM	100					
Index	HLW (COGEMA)		HLW (BNFL)		SF	
	Radius	Temperature	Radius	Temperature	Radius	Temperature
	[m]	[°C]	[m]	[°C]	[m]	[°C]
33	0.3025	52.76	0.3025	56.55	0.3575	54.30
34	0.305	52.75	0.305	56.54	0.36	54.29
35	0.3075	52.74	0.3075	56.53	0.3625	54.28
36	0.31	52.74	0.31	56.52	0.365	54.28
37	0.3125	52.73	0.3125	56.51	0.3675	54.27
38	0.315	52.72	0.315	56.51	0.37	54.26
39	0.3175	52.72	0.3175	56.50	0.3725	54.26
40	0.32	52.71	0.32	56.49	0.375	54.25
41	0.3225	52.70	0.3225	56.48	0.3775	54.25
42	0.325	52.70	0.325	56.47	0.38	54.24
43	0.3275	52.69	0.3275	56.47	0.3825	54.23
44	0.33	52.68	0.33	56.46	0.385	54.23
45	0.3325	52.68	0.3325	56.45	0.3875	54.22
46	0.335	52.67	0.335	56.44	0.39	54.22
47	0.3375	52.67	0.3375	56.43	0.3925	54.21
48	0.34	52.66	0.34	56.43	0.395	54.20
49	0.3425	52.65	0.3425	56.42	0.3975	54.20
50	0.345	52.65	0.345	56.41	0.4	54.19
51	0.3475	52.64	0.3475	56.40	0.4025	54.19
52	0.35	52.64	0.35	56.40	0.405	54.18
53	0.3525	52.63	0.3525	56.39	0.4075	54.18
54	0.355	52.62	0.355	56.38	0.41	54.17
55	0.3575	52.62	0.3575	56.37	0.4125	54.16
56	0.36	52.61	0.36	56.37	0.415	54.16
57	0.3625	52.61	0.3625	56.36	0.4175	54.15
58	0.365	52.60	0.365	56.35	0.42	54.15
59	0.3675	52.60	0.3675	56.34	0.4225	54.14
60	0.37	52.59	0.37	56.34	0.425	54.14
61	0.3725	52.59	0.3725	56.33	0.4275	54.13
62	0.375	52.58	0.375	56.32	0.43	54.13
63	0.3775	52.57	0.3775	56.32	0.4325	54.12
64	0.38	52.57	0.38	56.31	0.435	54.12
65	0.3825	52.56	0.3825	56.30	0.4375	54.11
66	0.385	52.56	0.385	56.30	0.44	54.11

C	0.82		1.05		0.92	
DELTAR	0.25					
NUM	100					
Index	HLW (COGEMA)		HLW (BNFL)		SF	
	Radius	Temperature	Radius	Temperature	Radius	Temperature
	[m]	[°C]	[m]	[°C]	[m]	[°C]
67	0.3875	52.55	0.3875	56.29	0.4425	54.10
68	0.39	52.55	0.39	56.28	0.445	54.09
69	0.3925	52.54	0.3925	56.27	0.4475	54.09
70	0.395	52.54	0.395	56.27	0.45	54.08
71	0.3975	52.53	0.3975	56.26	0.4525	54.08
72	0.4	52.53	0.4	56.25	0.455	54.07
73	0.4025	52.52	0.4025	56.25	0.4575	54.07
74	0.405	52.52	0.405	56.24	0.46	54.06
75	0.4075	52.51	0.4075	56.24	0.4625	54.06
76	0.41	52.51	0.41	56.23	0.465	54.05
77	0.4125	52.50	0.4125	56.22	0.4675	54.05
78	0.415	52.50	0.415	56.22	0.47	54.04
79	0.4175	52.49	0.4175	56.21	0.4725	54.04
80	0.42	52.49	0.42	56.20	0.475	54.03
81	0.4225	52.48	0.4225	56.20	0.4775	54.03
82	0.425	52.48	0.425	56.19	0.48	54.03
83	0.4275	52.47	0.4275	56.18	0.4825	54.02
84	0.43	52.47	0.43	56.18	0.485	54.02
85	0.4325	52.46	0.4325	56.17	0.4875	54.01
86	0.435	52.46	0.435	56.17	0.49	54.01
87	0.4375	52.45	0.4375	56.16	0.4925	54.00
88	0.44	52.45	0.44	56.15	0.495	54.00
89	0.4425	52.44	0.4425	56.15	0.4975	53.99
90	0.445	52.44	0.445	56.14	0.5	53.99
91	0.4475	52.43	0.4475	56.14	0.5025	53.98
92	0.45	52.43	0.45	56.13	0.505	53.98
93	0.4525	52.42	0.4525	56.13	0.5075	53.97
94	0.455	52.42	0.455	56.12	0.51	53.97
95	0.4575	52.42	0.4575	56.11	0.5125	53.97
96	0.46	52.41	0.46	56.11	0.515	53.96
97	0.4625	52.41	0.4625	56.10	0.5175	53.96
98	0.465	52.40	0.465	56.10	0.52	53.95
99	0.4675	52.40	0.4675	56.09	0.5225	53.95
100	0.47	52.39	0.47	56.09	0.525	53.94